Atmos. Chem. Phys., 25, 10293–10314, 2025
https://doi.org/10.5194/acp-25-10293-2025

Atmospheric Chemistry and Physics
Open Access

Incorporation of multi-phase halogen chemistry into the Community Multiscale Air Quality (CMAQ) model

Kiyeon Kim[1], Chul Han Song[1], Kyung Man Han[1], Greg Yarwood[2], Ross Beardsley[2], and Saewung Kim[3]

[1]Department of Environment and Energy Engineering, Gwangju Institute of Science and Technology (GIST), Gwangju 61005, Republic of Korea
[2]Ramboll, Novato, CA 94945, USA
[3]Department of Earth System Science, University of California, Irvine, CA, USA

Correspondence: Chul Han Song (chsong@gist.ac.kr)

Received: 3 January 2025 – Discussion started: 21 January 2025
Revised: 17 June 2025 – Accepted: 17 June 2025 – Published: 10 September 2025

Abstract. Halogen radicals (Cl, Br, and I) significantly influence atmospheric oxidation capacity, affecting both O_3 formation and destruction. However, understanding of halogen chemistry remains limited. To better investigate comprehensive atmospheric halogen chemistry, we incorporated halogen processes into the Community Multi-scale Air Quality (CMAQ) model: (i) emissions of Cl_2, HCl, Br_2, and HBr from anthropogenic sources and Br_2, I_2, HOI, and halocarbons from natural sources and (ii) 177 multi-phase halogen reactions. Model performance was evaluated against observed $ClNO_2$ levels and by comparison with reported ranges of BrO and IO levels. The updated model showed significant improvements in simulating $ClNO_2$ mixing ratios, with the index of agreement (IOA) increasing from 0.41 to 0.66 and mean bias (MB) decreasing from −159.36 to −25.07 ppt at supersites. Furthermore, simulated BrO and IO levels fell within the ranges reported in previous studies. We found that these improvements were driven by four key reactions: (i) ClO self-reaction, (ii) heterogeneous HOBr chemistry, (iii) NO_2 uptake, and (iv) revised N_2O_5 parameterization. Based on our modeling system, we found that the presence of halogen radicals led to changes in the net O_x production rate ($P(O_x)$), which increased from 3.08 to 3.33 ppb h^{-1} on land and decreased from 0.21 to 0.07 ppb h^{-1} over ocean. It was noted that levels of OH, HCHO, and NO_x also increased by ∼ 0.007 ppt (5.5 %), ∼ 0.03 ppb (1.6 %), and ∼ 0.29 ppb (2.9 %), respectively, while levels of HO_2 and volatile organic compounds (VOCs) decreased by ∼ 0.45 ppt (5.3 %) and ∼ 0.71 ppb (5.9 %). These results highlight the importance of accurately representing halogen processes in regional air quality models.

1 Introduction

Atmospheric oxidants, such as OH, NO_3, and O_3, play a significant role in atmospheric chemistry. These oxidants react with volatile organic compounds (VOCs), leading to the formation of peroxyl radicals (RO_2), which, in turn, influences the O_3 formation. They also contribute to the formation of secondary organic and inorganic aerosols. Meanwhile, halogen radicals (such as Cl, Br, and I) also serve as oxidants in the atmosphere, affecting the oxidation capacity through various reactions (Reactions R1–R4; see below) (Simpson et al., 2015; von Glasow and Crutzen, 2007; Fan and Li, 2022).

$$\mathrm{X\ (Cl, Br,\ and\ I)} + \mathrm{VOC} \rightarrow \mathrm{RO_2} \quad \text{(R1)}$$

$$\mathrm{RO_2} + \mathrm{NO} \rightarrow \mathrm{NO_2} + \mathrm{RO} \quad \text{(R2)}$$

$$\mathrm{HO_2} + \mathrm{NO} \rightarrow \mathrm{NO_2} + \mathrm{OH} \quad \text{(R3)}$$

$$\mathrm{NO_2} \xrightarrow{h\nu} \mathrm{O^{3p}} + \mathrm{O_2} \xrightarrow{\mathrm{M}} \mathrm{O_3} \quad \text{(R4)}$$

$$\mathrm{X} + \mathrm{O_3} \rightarrow \mathrm{XO} + \mathrm{O_2} \quad \text{(R5)}$$

$$\mathrm{XO} + \mathrm{HO_2} \rightarrow \mathrm{HOX} + \mathrm{O_2} \quad \text{(R6)}$$

$$\mathrm{HOX} \xrightarrow{h\nu} \mathrm{X} + \mathrm{OH} \quad \text{(R7)}$$

These radicals can also make substantial impacts on the O_3 loss via Reactions (R5)–(R7) (Saiz-Lopez et al., 2012; Sarwar et al., 2015; Simpson et al., 2015). Given their roles in both the O_3 formation and destruction, a comprehensive understanding of atmospheric halogen chemistry is essential for accurately assessing the oxidative potentials of the atmosphere.

In this context, several studies attempted to incorporate chlorine chemistry into chemical transport models (e.g., Yi et al., 2021; Sarwar et al., 2012; Qiu et al., 2019a, b). Specifically, Qiu et al. (2019a) reported that heterogeneous reactions involving reactive chlorine species can increase O_3 levels by approximately 20 %. Moreover, Liu et al. (2018) found that the mixing ratios of O_3 increased by ~ 7.7 ppbv when anthropogenic chlorine emissions were included.

On the other hand, numerous studies have emphasized not only the significance of chlorine chemistry but also the influence of the synergistic effects of bromine and iodine chemistry with chlorine chemistry (Sarwar et al., 2019; Simpson et al., 2015; Caram et al., 2023; Badia et al., 2019; Saiz-Lopez et al., 2014; Li et al., 2022; Iglesias-Suarez et al., 2020). For instance, modeling studies considering both bromine and iodine chemistries showed that simulated O_3 levels actually decreased by 15.9 ppb (Parrella et al., 2012; Sarwar et al., 2015; Herrmann et al., 2022; Gantt et al., 2017; Read et al., 2008; Huang et al., 2021). These findings strongly suggest that incorporating chlorine processes, together with bromine and iodine processes, is crucial for correct and comprehensive understanding of atmospheric chemistry.

The Korean Peninsula, surrounded by the Yellow Sea, Korea Strait, and the East Sea, is characterized by high population density and highly industrial regions. Therefore, it can be influenced by both natural (oceanic) and anthropogenic halogen emissions. However, almost no modeling study has taken into account the natural and anthropogenic halogen processes over/around South Korea. Although almost no research has been carried out to examine the impacts of halogen chemistry on atmospheric composition over/around South Korea, several studies have considered atmospheric chlorine processes using 3D chemical transport models (CTMs) (e.g., Jo et al., 2023; Kim et al., 2023). Given the synergistic effects of chlorine, bromine, and iodine chemistries in the atmosphere, a comprehensive study that takes all these halogen processes into account is absolutely necessary.

For the comprehensive analysis of halogen processes and their influence on regional air quality, we established anthropogenic and natural halogen emissions and incorporated full sets of halogen reactions into the framework of the Community Multi-scale Air Quality (CMAQ) model. Specifically, we incorporated the following halogen processes into the CMAQ model: (i) atmospheric chlorine processes (anthropogenic HCl and Cl_2 emissions with 58 chlorine reactions), (ii) atmospheric bromine processes (anthropogenic and natural HBr and Br_2 emissions together with 64 bromine reactions), and (iii) atmospheric iodine processes (HOI and I_2 natural emissions, along with 55 iodine reactions).

Based on this modeling system, the primary objectives of this study are threefold: (i) to develop and implement an updated halogen chemistry that accounts for the interactions among multiple halogen species; (ii) to evaluate model performance using observational data from the Korea US Air Quality (KORUS-AQ) campaign (1 May–12 June 2016), including direct $ClNO_2$ measurements and inferred estimates of BrO and IO; and (iii) to examine the atmospheric impacts of the updated halogen chemistry on a broader set of key atmospheric constituents such as O_3, OH, HO_2, HCHO, VOC_s, and NO_x. In this context, this study is designed to support a comprehensive understanding of atmospheric halogen processes and their implications for regional air quality.

2 Methodology

In this study, we incorporated homogeneous, aqueous, and heterogeneous halogen reactions into the CMAQ model, along with emissions of halogen species. To evaluate the accuracy of these halogen processes, we compared the model results with observational data from the KORUS-AQ campaign (Jeong et al., 2019; Crawford et al., 2021). This section provides several details on the observation data, the WRF-CMAQ model configurations, and the atmospheric halogen processes, including halogen reactions and emissions.

2.1 Observation data

Mixing ratios of nitryl chloride ($ClNO_2$) were measured every 5 min at Olympic Park (37.52° N; 127.12° E) and Mount Taehwa (37.27° N; 127.41° E) stations during the period of the KORUS-AQ campaign (refer to two blue stars in Fig. 1a), using the Chemical Ionization Mass Spectrometer (CIMS). The CIMS instrument has a detection limit of 1.5 ppt and an uncertainty within 20 %. Further details on the CIMS instrument are found in Slusher et al. (2004) and Jeong et al. (2019). In our study, $ClNO_2$ observations were utilized to evaluate the performance of the modified CMAQ model simulations. These results are discussed in Sect. 3.1.

2.2 WRF-CMAQ model description

The Weather Research and Forecasting (WRF) v3.8.1 model simulations were carried out to generate meteorological fields (Skamarock et al., 2008). The details of physical parameters used in the WRF simulations are summarized in Table S1 in the Supplement. National Center for Environmental Prediction Final Analysis (NCEP-FNL) data were used for initial and boundary conditions. The WRF model included a 5 d spin-up period to minimize uncertainties from the initial and boundary conditions.

This study also included the CMAQ v5.2.1 model simulations (Byun and Schere, 2006) over a domain covering

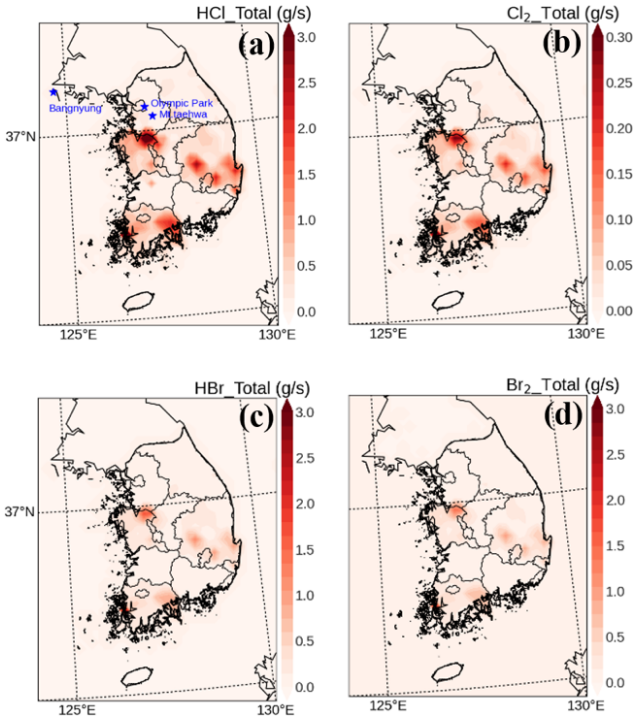

Figure 1. Spatial distributions of anthropogenic emission rates of **(a)** HCl, **(b)** Cl_2, **(c)** HBr, and **(d)** Br_2 during the period of the KORUS-AQ campaign over South Korea. Three blue stars denote the locations of three supersites (Bangnyung, Olympic Park, and Mount Taehwa) during the KORUS-AQ campaign.

northeast Asia with 273 × 204 horizontal grid cells. The grid resolution is 15 km × 15 km with 15 vertical layers from surface to 50 hPa. The Statewide Air Pollution Research Center-07 (SAPRC-07TC) mechanism (Carter, 2010; Hutzell et al., 2012) with AERO6 module was used in the CMAQ model simulations. One limitation of the SAPRC-07TC mechanism is that it has only basic chlorine chemistry. In order to implement more sophisticated halogen model simulations, we incorporated additional and updated halogen reactions into the SAPRC-07TC mechanism. The detailed reactions are explained in Sect. 2.4.1 and 2.4.2.

In order to run the CMAQ model, biomass burning and biogenic emissions were obtained from the Fire Inventory from NCAR (FINN) v1.5 (Wiedinmyer et al., 2011) and the Model of Emissions of Gases and Aerosol from Nature (MEGAN) v2.1 (Guenther et al., 2012), respectively. Anthropogenic emissions were acquired from the KORUS v5.0 emission inventory (Woo et al., 2020), specifically developed for the KORUS-AQ campaign. The KORUS v5.0 inventory covers emissions of primary pollutants such as NO_x, CO, HCHO, VOCs, and particulate chlorine (pCl^-), but it omits the emissions for anthropogenic chlorine species (HCl and Cl_2), bromine species (HBr and Br_2), and ocean-generated halogen species (HOI, I_2, and halocarbons). We have thus developed new halogen emissions for this study. The methodology for developing the halogen emissions will be discussed in Sect. 2.3.1 and 2.3.2.

2.3 Halogen emissions

In this section, we discuss the development of anthropogenic and natural halogen emissions within our model framework.

2.3.1 Anthropogenic emissions

First, we assumed that emissions of anthropogenic HCl and Cl_2 mainly originated from coal combustion. Coal combustion occurs predominantly in four main sectors: industry, residential areas, power plants, and other sectors such as agriculture and furniture manufacturing. In addition, HCl emissions also take place from municipal solid waste incineration.

To calculate chlorine emissions from industry and residential areas, we utilized coal consumption data from the 2016 Regional Energy Report of South Korea (https://www.keei.re.kr, last access: 19 August 2025). Thereafter, the emissions of HCl and Cl_2 from these sectors were calculated using Eq. (1):

$$E_{i,j} = M_{i,j} \times \mathrm{EF}_{i,j} \times \rho \times \frac{1}{\mathrm{MM}} \times \frac{1}{10^3}, \quad (1)$$

where $E_{i,j}$ represents the emission for species i in categories j (Mg); M denotes the coal consumption (Gg); and EF is the emission factor ($\mu g\, g^{-1}$) calculated using the method from a previous study (Jiang et al., 2005). ρ indicates the percentage of HCl and Cl_2 in the chlorine content of coal. In our study, percentages of 86.3 % and 3.63 % for ρ_{HCl} and ρ_{Cl_2} were used, respectively, based on research conducted by Deng et al. (2014) and Liu et al. (2018). MM represents the ratios of the molar mass of the chlorine atom to the molecular weight (i.e., 35.5/36.5 for HCl and 1 for Cl_2).

For the remaining three sectors, namely power plants, solid waste incineration, and others, the HCl emissions were obtained directly from the Korean tele-monitoring system (TMS) named the CleanSYS (https://cleansys.or.kr, last access: 19 August 2025). Meanwhile, the emissions of Cl_2 from these sectors can also be calculated using Eq. (1), based on the HCl emissions previously calculated.

Bromine emissions (HBr and Br_2) were additionally estimated from the previously calculated chlorine emissions. According to a recent study, bromine is also emitted from the coal combustion with a ratio (0.25) of bromine to chlorine concentrations (Peng and Wu, 2014). These bromine emissions were split into 70 % and 30 % for HBr and Br_2, respectively. The detailed methodology used in our study is summarized in Li et al. (2021).

Consequently, we developed an emission inventory that includes anthropogenic chlorine and bromine emissions. Figure 1 illustrates the spatial distributions of these emissions across South Korea. The total emission rates for anthropogenic HCl, Cl_2, HBr, and Br_2 in South Korea are 5989.6,

450.8, 460.8, and 240.8 Mg yr^{-1}, respectively. These values are higher than those reported in previous studies conducted for the same region and time period. For instance, Jo et al. (2023) estimated that total annual anthropogenic HCl emissions were less than 1.0 Gg, whereas Kim et al. (2023) reported a value of 1.35 Gg. These discrepancies may result from the inclusion of additional HCl emissions from the residential and industrial sectors in our study. Moreover, our research also accounts for emissions of Cl_2, HBr, and Br_2. It is noteworthy that Cl_2, HBr, and Br_2 have relatively shorter *e*-folding lifetimes (a few minutes for Cl_2 and Br_2, and a few hours for HBr) than HCl (about 1.5 d), which may increase the oxidant capacity in the atmosphere.

2.3.2 Natural emissions

Biogenic halocarbons, such as $CHBr_3$, CH_2Br_2, $CHBrCl_2$, CH_2BrCl, $CHBr_2Cl$, CH_2I_2, CH_3I, CH_2ICl, and CH_2IBr, are emitted from micro-algae activities in the ocean. To calculate these emissions of bromine- and iodine-containing halocarbon species, we used the chlorophyll *a* (chl *a*) concentrations as a proxy for the photosynthetic activity of phytoplankton (Liss et al., 2014).

Chlorophyll *a* concentrations in the ocean have been monitored by various satellite sensors such as the Moderate Resolution Imaging Spectroradiometer (MODIS) and the Geostationary Ocean Color Imager (GOCI) (Kim et al., 2016; O'Reilly and Werdell, 2019; Sarwar et al., 2015). Among these sensors, Park et al. (2015) reported that the chlorophyll *a* concentrations measured by the GOCI sensor showed the best agreement with surface observations compared to those from the MODIS sensor in the East Asian ocean. Based on this study, we applied the chlorophyll *a* data from the GOCI sensor into our study (refer to Fig. S1 in the Supplement).

Gridded halocarbon emissions were estimated using Eq. (2) (Sarwar et al., 2015):

$$E_{\text{Halocarbon}} = 1.2 \times 10^{-11} \times (O_F + S_F) \times A_{GC} \times f_{HC} \times f_{DP} \times [\text{chl } a], \quad (2)$$

where O_F and S_F represent the ocean and coastal fractions of the grid cell, respectively. A_{GC} denotes the area of the grid cell (m^2). f_{HC} is the emission factor for the species, and f_{DP} represents the diurnal profile. [chl *a*] denotes the chlorophyll *a* concentration. The distributions of natural bromine and iodine emissions are shown in Fig. S2.

Natural Br_2 emissions were estimated by debromination of sea salt aerosols (SSAs), following the method proposed by Sarwar et al. (2015) and Yang et al. (2005). In this approach, Br^- contained within the SSAs was released into the atmosphere as Br_2 (i.e., dehalogenation of SSAs). This process was parameterized based on sea salt aerosol mass, Br/NaCl mass ratio, sea surface temperature, and 10 m wind speed. In addition, inorganic iodine (such as HOI and I_2) emissions were calculated at the air–sea water interfaces, utilizing information on dry deposition of O_3 over the ocean. This approach is based on the fact that the formations of HOI and I_2 are initiated by reaction between iodide (I^-(aq)) and O_3 at the ocean surfaces. More detailed information on natural inorganic emissions can be found in Sarwar et al. (2015).

2.4 Halogen chemical reactions

As mentioned previously, the conventional CMAQ v5.2.1 model accounts for only a limited set of chlorine-related processes: (i) reactions between VOCs and Cl radicals (Sander et al., 2010), (ii) a simplified reactive chlorine cycling mechanism (Sander et al., 2010), and (iii) the uptake of N_2O_5 on the chloride-containing particles (Bertram and Thornton, 2009). Therefore, we attempted to incorporate the multi-phase halogen reactions into the CMAQ v5.2.1 model to investigate the influences of atmospheric halogen chemistry. Detailed descriptions of these reactions are provided in the subsequent sections.

2.4.1 Chlorine reactions

The chlorine-related reactions were incorporated into the framework of SAPRC07-TC mechanism. The chlorine reactions consist of (i) adjusted reaction rate coefficients for 14 reactions (refer to Reactions R9–R22 in Table 1); (ii) updated 29 gaseous chlorine reactions (refer to Reactions R23–R51 in Table 1); (iii) added two aqueous-phase reactions (refer to Reactions R1 and R2 in Table 2); and (iv) incorporated four heterogeneous reactions involving three reactive halogen species, HOCl, $ClNO_2$, and $ClONO_2$, with NO_2 partitioning onto chloride-containing particles (refer to Reactions R2–R6 in Table 3).

The parameterization of $\gamma_{N_2O_5}$ currently embedded in the CMAQ v5.2.1 model (shown in Reaction R8) has not been greatly satisfactory for reproducing the atmospheric levels of $ClNO_2$.

$$N_2O_5 + (1-\varphi)H_2O + \varphi Cl^{-1} \xrightarrow{\gamma_{N_2O_5}} (2-\varphi)HNO_3 + \varphi ClNO_2, \quad (R8)$$

where φ represents the yield of $ClNO_2$ as a function of the concentration of particulate chloride [Cl^-] and aerosol water content [H_2O]. The calculation of φ was proposed by Bertram and Thornton (2009):

$$\varphi = \frac{1}{1 + \frac{[H_2O]}{483[Cl^-]}}. \quad (3)$$

Although the use of Reaction (R8) and Eq. (3) has been an advance in considering the production of $ClNO_2$ from chlorine-containing particles (Bertram and Thornton, 2009), several studies have reported that the parameterizations of $\gamma_{N_2O_5}$ with Reaction (R8) and Eq. (3) tend to produce excessive amounts of nitrate and $ClNO_2$ (Riedel et al., 2012b;

Table 1. List of homogeneous chlorine reactions used in this study.

No.	Reaction	Reaction rate	Reference
R1	$Cl_2 \xrightarrow{h\nu} 2Cl$	#1.0/ <Cl_2>	1
R2	$ClNO \xrightarrow{h\nu} Cl + NO$	#1.0/ <ClNO>	1
R3	$Cl + NO_2 + M = ClONO$	$k_0 = 1.3 \times 10^{-30}(T/300)^{-2.0}$, $k_\infty = 1.0 \times 10^{-10}(T/300)^{-1.0}$, $F = 0.6$ and $N = 1.0$	1
R4	$Cl + NO_2 + M = ClNO_2$	$k_0 = 1.8 \times 10^{-31}(T/300)^{-2.0}$, $k_\infty = 1.0 \times 10^{-10}(T/300)^{-1.0}$, $F = 0.6$ and $N = 1.0$	1
R5	$ClONO \xrightarrow{h\nu} Cl + NO_2$	#1.0/ <ClONO>	1
R6	$Cl + NO_3 = ClO + NO_2$	2.4×10^{-11}	1
R7	$ClO + NO_2 = ClONO_2$	$k_0 = 1.8 \times 10^{-31}(T/300)^{-3.4}$, $k_\infty = 1.5 \times 10^{-11}(T/300)^{-1.9}$, $F = 0.6$ and $N = 1.0$	1
R8	$HOCl \xrightarrow{h\nu} Cl + OH$	#1.0/ <HOCl>	1
R9	$ClONO_2 = Cl + NO_3$	#1.0/ <$ClONO_{2\_1}$>	2
R10	$ClONO_2 = ClO + NO_2$	#1.0/ <$ClONO_{2\_2}$>	2
R11	$Cl + NO + M = 2ClNO$	$7.70 \times 10^{-32}\left(\frac{T}{300}\right)^{-1.8}$	2
R12	$ClNO_2 \xrightarrow{h\nu} Cl + NO_2$	#1.0/ <$ClNO_2$>	2
R13	$Cl + HO_2 = HCl$	$1.4 \times 10^{-11} e^{270/T}$	2
R14	$Cl + HO_2 = ClO + OH$	$3.6 \times 10^{-11} e^{-375/T}$	2
R15	$Cl + O_3 = ClO$	$2.3 \times 10^{-11} e^{200/T}$	2
R16	$ClO + NO = Cl + NO_2$	$6.4 \times 10^{-12} e^{290/T}$	2
R17	$ClONO_2 = ClO + NO_2$	2.0×10^{-21}	2
R18	$Cl + ClONO_2 = Cl_2 + NO_3$	$6.5 \times 10^{-12} e^{135/T}$	2
R19	$ClO + HO_2 = HOCl$	$2.6 \times 10^{-12} e^{290/T}$	2
R20	$ClO + ClO = Cl_2 + O_2$	$1.0 \times 10^{-11} e^{-1590/T}$	2
R21	$OH + HCl = Cl$	$1.8 \times 10^{-12} e^{-250/T}$	2
R22	$Cl + H_2 = HCl + HO_2$	$3.1 \times 10^{-11} e^{-2270/T}$	2
R23	$ClO + O = Cl + O_2$	$2.8 \times 10^{-11} e^{85/T}$	2
R24	$ClO + OH = Cl + HO_2$	$7.4 \times 10^{-12} e^{270/T}$	2
R25	$ClO + OH = HCl + O_2$	$6.0 \times 10^{-13} e^{230/T}$	2
R26	$HOCl + OH = ClO + H_2O$	$3.0 \times 10^{-12} e^{-500/T}$	2
R27	$HOCl + O = ClO + OH$	1.7×10^{-13}	2
R28	$ClNO_2 + OH = HOCl + NO_2$	$2.4 \times 10^{-12} e^{-1250/T}$	2
R29	$ClONO_2 + O = ClO + NO_3$	$3.6 \times 10^{-12} e^{-840/T}$	2
R30	$ClONO_2 + OH = HOCl + NO_3$	$1.2 \times 10^{-12} e^{-330/T}$	2
R31	$HCl + O = Cl + OH$	$1.0 \times 10^{-11} e^{-3300/T}$	2
R32	$Cl + ClNO = NO + Cl_2$	$5.8 \times 10^{-11} e^{100/T}$	2
R33	$Cl + HOCl = OH + Cl_2$	$3.4 \times 10^{-12} e^{-130/T}$	2
R34	$ClO \xrightarrow{h\nu} Cl + O$	#1.0/ <ClO>	2
R35	$Cl + H_2O_2 = HCl + HO_2$	$1.1 \times 10^{-11} e^{-980/T}$	2
R36	$OH + Cl_2 = HOCl + Cl$	$2.6 \times 10^{-12} e^{-1100/T}$	2
R37	$Cl + HNO_3 = HCl + NO_2$	2.0×10^{-16}	2
R38	$Cl_2O_2 \xrightarrow{h\nu} Cl + ClO_2$	#1.0/ <Cl_2O_2>	2
R39	$ClO_2 \xrightarrow{h\nu} ClO + O_2$	#1.0/ <ClO_2>	2
R40	$Cl + ClO_2 = 2ClO$	1.2×10^{-11}	2
R41	$Cl + ClO_2 = Cl_2 + O_2$	2.3×10^{-10}	2
R42	$OH + Cl_2O_2 = HOCl + ClO_2$	$6.0 \times 10^{-13} e^{670/T}$	2
R43	$OH + ClO_2 = HOCl + O_2$	$1.4 \times 10^{-12} e^{600/T}$	2
R44	$Cl + O_2 + M = ClO_2$	$k_0 = 2.2 \times 10^{-33}(T/300)^{-3.1}$, $k_\infty = 1.8 \times 10^{-10}(T/300)^{0.0}$, $F = 0.6$ and $N = 1.0$	2
R45	$ClO + ClO + M = ClO_2$	$k_0 = 1.9 \times 10^{-32}(T/300)^{-3.6}$, $k_\infty = 3.7 \times 10^{-12}(T/300)^{-1.6}$, $F = 0.6$ and $N = 1.0$	2
R46	$ClO_2 + O = ClO$	$2.4 \times 10^{-12} e^{-960/T}$	2
R47	$NO + ClO_2 = ClO + NO_2$	$6.0 \times 10^{-13} e^{-670/T}$	2
R48	$HCl + NO_3 = HNO_3 + Cl$	5.0×10^{-17}	2
R49	$Cl + Cl_2O_2 = Cl_2 + ClO$	$6.2 \times 10^{-11} e^{130/T}$	2
R50	$ClO + O_3 = ClO_2$	$2.0 \times 10^{-12} e^{-3600/T}$	2
R51	$ClO + NO_3 = ClO_2 + NO_2$	4.7×10^{-13}	2

1 – Sander et al. (2010); 2 – Burkholder et al. (2020).

Table 2. List of aqueous-phase chlorine and bromine reactions used in this study.

No.	Species	Reaction	Reaction rate (unit: $M\,s^{-1}$)	Reference
R1	HOCl	$HOCl + HSO_3^- \xrightarrow{k} SO_4^{2-} + Cl^- + 2H^+$	2.8×10^5	1
R2	HOCl	$HOCl + SO_3^{2-} \xrightarrow{k} SO_4^{2-} + HCl$	7.6×10^8	1
R3	HOBr	$HOBr + HSO_3^- \xrightarrow{k} SO_4^{2-} + HBr$	5.0×10^9	1
R4	HOBr	$HOBr + SO_3^{2-} \xrightarrow{k} SO_4^{2-} + HBr$	2.6×10^7	1

1 – Liu and Abbatt (2020).

Table 3. List of heterogeneous halogen reactions and the uptake coefficients of gases used in this study.

No.	Gas	Reaction	Uptake coefficient (γ_{gas})	Reference
R1	N_2O_5	$N_2O_5 + (1-\varphi)H_2O + \varphi Cl^- \rightarrow (2-\varphi)HNO_3 + \varphi ClNO_2$	Function of aerosol mass concentrations, relative humidity, and temperature	1, 2
R2	HOCl	$HOCl + Cl^- = Cl_2$	1.09×10^{-3}	3
R3	$ClONO_2$	$ClONO_2 + Cl^- = Cl_2 + NO_3^-$	0.002	4
R4	$ClNO_2$	$ClNO_2 + Cl^- + H^+ = Cl_2 + HONO$	2.65×10^{-6} (pH < 2.0)	5
R5	$ClNO_2$	$ClNO_2 = Cl^- + NO_3^- + 2H^+$	6×10^{-6} (pH > 2.0)	6
R6	NO_2	$2NO_2 + Cl^- = ClNO + NO_3^-$	10^{-4}	7
R7	HOBr	$HOBr + Br^- = Br_2$	0.08	8
R8	HOBr	$HOBr + Cl^- = BrCl$	0.02	8
R9	$BrONO_2$	$BrONO_2 + H_2O = HOBr + HNO_3$	0.03	9
R10	HBr	$HBr = Br^-$	$1.3 \times 10^{-8} e^{\frac{4290}{T}}$	10
R11	$IONO_2$	$IONO_2 + Cl^- = ICl + HNO_3$	0.005	11
R12	$IONO_2$	$IONO_2 + Br^- = IBr + HNO_3$	0.005	11
R13	INO_2	$INO_2 + Cl^- = ICl + HONO$	0.01	11
R14	INO_2	$INO_2 + Br^- = IBr + HONO$	0.01	11
R15	HOI	$HOI + Cl^- = ICl$	0.005	12
R16	HOI	$HOI + Br^- = IBr$	0.005	12
R17	I_2O_2	$I_2O_2 =$	0.02	12
R18	I_2O_3	$I_2O_3 =$	0.02	12
R19	I_2O_4	$I_2O_4 =$	0.02	12

1– Riemer et al. (2003); 2 – Evans and Jacob (2005); 3 – Pratte and Rossi (2006); 4 – Chen et al. (2022); 5 – Riedel et al. (2012a); 6 – Roberts et al. (2009); 7 – Abbatt and Waschewsky (1998); 8 – Fernandez et al. (2014); 9 – Deiber et al. (2004); 10 – Ammann et al. (2013); 11 – Saiz Lopez et al. (2014); 12 – Sherwen et al. (2016).

Li et al., 2016; Yu et al., 2020). This overestimation may result from uncertainties in calculating aerosol water content ($[H_2O]$) estimated from the aerosol thermodynamic module (Chang et al., 2016). To deal with this issue, several studies have explored different parameterizations of $\gamma_{N_2O_5}$. However, the $\gamma_{N_2O_5}$ still appears to be over-estimated in many cases (e.g., Chang et al., 2016; Liu et al., 2019; McDuffie et al., 2018; Riedel et al., 2012b; Wang et al., 2017). In this context, we alternatively selected a different parameterization for $\gamma_{N_2O_5}$ (see Eqs. 4–7). These parameterizations were suggested by Riemer et al. (2003) and Evans and Jacob (2005):

$$\gamma_{N_2O_5} = f \times \gamma_1 + (1-f) \times \gamma_2 \quad (4)$$

$$f = \frac{m_{\text{sulfate}}}{m_{\text{sulfate}} + m_{\text{nitrate}}} \quad (5)$$

$$\gamma_1 = \alpha \times 10^{\beta} \quad (6)$$

$$\gamma_2 = 0.1 \times \gamma_1, \quad (7)$$

where α is set to be $2.79 \times 10^{-4} + 1.3 \times 10^{-4} \times RH - 3.43 \times 10^{-4} \times RH^2 + 7.52 \times 10^{-8} \times RH^3$. β is set at 0.48, when $T < 282$ K, or at $4 \times 10^{-2} \times (294 - T)$, when $T \geq 282$ K. m_i represents the aerosol mass concentration of species i. Complete lists of chlorine reactions embedded into the SAPRC07TC mechanism are shown in Tables 1–3.

2.4.2 Bromine reactions

We also incorporated bromine reactions into the SAPRC07-TC mechanism. The reactions incorporated include the following: (i) updated absorption cross-sections for BrCl, BrCHO, $CHBr_2Cl$, $CHBr_3$, and $CHBrCl_2$ (refer to Reactions R29–R33 in Table 4); (ii) updated reaction rates for formaldehyde (HCHO) and acetaldehyde (CH_3CHO) react-

ing with bromine radicals (refer to Reactions R34 and R35 in Table 4); (iii) Br-initiated VOC reactions (refer to Reactions R36–R56 in Table 4); (iv) two inter-halogen species reactions (refer to Reactions R57 and R58 in Table 4); (v) two aqueous-phase reactions (refer to Reactions R3 and R4 in Table 2); and (vi) four heterogeneous reactions for bromine species (refer to Reactions R7–R10 in Table 3). A complete list of the bromine reactions can be found in Tables 2–4.

2.4.3 Iodine reactions

Iodine reactions taken into account in this study were acquired from Saiz-Lopez et al. (2014) and Sherwen et al. (2016). We updated iodine reactions in three ways: (i) updated absorption cross-sections for ICl and IBr (refer to Reactions R43 and R44 in Table 5); (ii) two inter-halogen species reactions (refer to Reactions R45 and R46 in Table 5); and (iii) nine heterogeneous reactions for $IONO_2$, INO_2, HOI, I_2O_2, I_2O_3, and I_2O_4 (refer to Reactions R11–R19 in Table 3). These iodine reactions are shown in Tables 3 and 5.

2.5 Experimental design

To better understand the impacts of atmospheric halogen chemistry, we designed four experiments: (i) experiment without halogen chemistry (referred to as CTRL); (ii) original CMAQv5.2.1 model simulation only with chlorine processes (EXP_{Cl}); (iii) experiment with both chlorine and bromine processes (EXP_{Cl_Br}); and (iv) experiment with full halogen processes ($EXP_{Cl\_Br\_I}$). The design of these four experiments is explained in Table 6.

In addition, in order to further analyze our results, we carried out two more experiments: (i) CMAQ model runs with the halogen chemistry constructed by Saiz-Lopez et al. (2014) (labeled as EXP_{CAM}) and (ii) CMAQ model run with the halogen chemistry constructed by Sarwar et al. (2015) (labeled as EXP_{CMAQ}). The former halogen chemistry was included in a global CTM named CAM-Chem, while the latter was in the CMAQ model. That is why we labeled these two experiments EXP_{CAM} and EXP_{CMAQ}, respectively.

3 Results and discussions

In this section, we discuss the accuracy of new halogen chemistry and processes through the comparison between simulated and measured mixing ratios of halogen-containing compounds during the period of the KORUS-AQ campaign. We then analyze the experimental results to evaluate the impacts of atmospheric halogen chemistry and processes on key-species concentrations in the atmosphere.

3.1 Model performances

3.1.1 Observed vs. modeled $ClNO_2$ mixing ratios

To evaluate the model performances, we used the mixing ratios of $ClNO_2$ observed at two supersites (Olympic Park and Mount Taehwa stations) in South Korea. Although the mixing ratios of atmospheric Cl_2 were also measured at these two stations, we focused solely on $ClNO_2$ observations due to several uncertainties associated with the Cl_2 analysis. These issues will be discussed later in Sect. 3.1.3.

Figure 2 presents the diurnal variations of modeled and observed mixing ratios of $ClNO_2$ at two monitoring stations. The CTRL simulation (black circles and lines in Fig. 2) and EXP_{CAM} (purple circles and lines in Fig. 2) could not reproduce the observed mixing ratios of $ClNO_2$ at the two supersites. For instance, the average mixing ratios of $ClNO_2$ at both monitoring stations were 0.00 ppt for CTRL and 15.40 ppt for EXP_{CAM}, while the observed average mixing ratio of $ClNO_2$ was 122.67 ppt. This large discrepancy may be primarily due to the absence of heterogeneous $ClNO_2$ formation via N_2O_5 in the halogen scheme implemented for EXP_{CAM}, which was based on Saiz-Lopez et al. (2014). It is noted that this mechanism was originally designed for clean, oceanic environments and does not account for anthropogenic chlorine sources or inland $ClNO_2$ formation pathways, such as the reactions of N_2O_5 with particulate chloride (recall Reaction R8: $N_2O_5 + (1-\varphi)H_2O + \eta Cl^- \rightarrow (2-\varphi)HNO_3 + \varphi ClNO_2$). To address these limitations, recent versions of the model have incorporated the previously missing pathways for HCl and $ClNO_2$ production (Li et al., 2022).

On the other hand, the EXP_{CMAQ} (blue circles and lines in Fig. 2) and $EXP_{Cl\_Br\_I}$ (red circles and lines in Fig. 2), which accounted for halogen chemistry, tend to better capture the diurnal patterns of observed mixing ratios of $ClNO_2$ (refer to open circles and lines in Fig. 2). These models also demonstrated significant improvements, in terms of statistical metrics (which will be presented in Table 7).

Although the EXP_{CMAQ} showed reasonable agreement, it also exhibited significant biases during the nighttime. Conversely, the $EXP_{Cl\_Br\_I}$ simulation achieved better agreement with the observed mixing ratios of $ClNO_2$ at both stations. For example, the index of agreement (IOA) increased from 0.62 for EXP_{CMAQ} to 0.66 for $EXP_{Cl\_Br\_I}$ and from 0.57 to 0.59 at Olympic Park and Mount Taehwa stations, respectively. These enhancements suggest that successful implementation of the models depends on not only considering chlorine reactions but also incorporating more comprehensive halogen reactions, as demonstrated by $EXP_{Cl\_Br\_I}$. The following sections will explore and discuss these halogen reactions in the atmosphere.

3.1.2 Contributions to mixing ratios of $ClNO_2$

Figure 3a and c represent the diurnal variations in the mixing ratios of $ClNO_2$ from the EXP_{CMAQ} (blue dotted line)

Table 4. List of homogeneous bromine reactions used in this study.

No.	Reaction	Reaction rate	Reference
R1	$BrO \xrightarrow{h\nu} Br + O^3P$	#1.0/ <BrO>	1
R2	$HOBr \xrightarrow{h\nu} Br + OH$	#1.0/ <HOBr>	1
R3	$BrNO_3 \xrightarrow{h\nu} Br + NO_3$	#1.0/ <$BrNO_3$_1>	1
R4	$BrNO_3 \xrightarrow{h\nu} BrO + NO_2$	#1.0/ <$BrNO_3$_2>	1
R5	$BrNO_2 \xrightarrow{h\nu} Br + NO_2$	#1.0/ <$BrNO_2$>	1
R6	$Br_2 \xrightarrow{h\nu} 2Br$	#1.0/ <Br_2>	1
R7	$Br + O_3 = BrO$	$1.6 \times 10^{-11} e^{-780/T}$	1
R8	$BrO + HO_2 = HOBr$	$4.5 \times 10^{-12} e^{460/T}$	1
R9	$Br + HO_2 = HBr$	$4.8 \times 10^{-12} e^{-310/T}$	1
R10	$HBr + OH = Br$	$5.5 \times 10^{-12} e^{200/T}$	1
R11	$BrO + BrO = 2Br$	$2.4 \times 10^{-12} e^{40/T}$	1
R12	$BrO + BrO = Br_2$	$2.8 \times 10^{-14} e^{860/T}$	1
R13	$BrO + NO = Br + NO_2$	$8.8 \times 10^{-12} e^{260/T}$	1
R14	$Br + BrNO_3 = Br_2 + NO_3$	4.9×10^{-11}	1
R15	$Br_2 + OH = HOBr + Br$	$2.1 \times 10^{-11} e^{240/T}$	1
R16	$BrO + OH = Br + HO_2$	$1.7 \times 10^{-11} e^{250/T}$	1
R17	$Br + NO_3 = BrO + NO_2$	1.6×10^{-11}	1
R18	$BrO + ClO = Br + Cl$	$4.7 \times 10^{-12} e^{320/T}$	1
R19	$BrO + MEO2 = 0.8HOBR + 0.2BR + 0.3HCOOH + 0.2HCHO + 0.13OH + 0.13HO_2$	$2.65 \times 10^{-14} e^{1600/T}$	1
R20	$CH_3Br + OH = Br$	$1.42 \times 10^{-12} e^{-1150/T}$	1
R21	$MB3^a + OH = 3Br$	$9.0 \times 10^{-13} e^{-360/T}$	1
R22	$MB2^b + OH = 2Br + HO_2$	$2.0 \times 10^{-12} e^{-840/T}$	1
R23	$MB2C^c + OH = 2Br + Cl$	$9.0 \times 10^{-13} e^{-420/T}$	1
R24	$MBC2^d + OH = Br + 2Cl$	$9.4 \times 10^{-13} e^{-510/T}$	1
R25	$MBC2^e + OH = Br + Cl + HO_2$	$2.1 \times 10^{-12} e^{-880/T}$	1
R26	$DMS + BrO = 0.75SO_2 + 0.25MSA + MEO2 + Br$	$1.5 \times 10^{-14} e^{1000/T}$	1
R27	$BrO + NO_2 = BrNO_3$	$k_0 = 5.2 \times 10^{-31}(T/300)^{-3.2}$, $k_\infty = 6.9 \times 10^{-12}(T/300)^{-2.9}$, $F = 0.6$ and $N = 1.0$	1
R28	$Br + NO_2 = BrNO_2$	$k_0 = 4.2 \times 10^{-31}(T/300)^{-2.4}$, $k_\infty = 2.7 \times 10^{-11}(T/300)^{0.0}$, $F = 0.6$ and $N = 1.0$	1
R29	$BrCl \xrightarrow{h\nu} Br + Cl$	#1.0/ <BrCl>	2
R30	$FMBR^f \xrightarrow{h\nu} Br + CO + HO_2$	# 1.0/ <FMBR>	2
R31	$MB3^a \xrightarrow{h\nu} 3.0Br + HO_2$	#1.0/ <MB3>	2
R32	$MB2C^c \xrightarrow{h\nu} 2.0Br + Cl + HO_2$	#1.0/ <MB2C>	2
R33	$MBC2^d \xrightarrow{h\nu} Br + 2.0Cl + HO_2$	#1.0/ <MBC2>	2
R34	$HCHO + Br = HBr + HO_2$	$7.7 \times 10^{-12} e^{-580/T}$	2
R35	$CCHO + Br = HBr + MECO_3$	$1.8 \times 10^{-11} e^{-460/T}$	2
R36	$ETHE + Br = FMBR^f + HCHO + HO2 + RO2C$	1.3×10^{-13}	2
R37	$OLE1 + Br = FMBR^f + CCHO + HO2 + RO2C$	3.6×10^{-12}	2
R38	$OLE2 + Br = FMBR^f + 0.75RCHO + 0.15ACET + 0.1MEK + HO2 + RO2C$	1.0×10^{-11}	2
R39	$ISOPRENE + Br = FMBR^f + PRD2 + HO2 + RO2C$	7.5×10^{-11}	2
R40	$FMBR^f + OH = Br + CO$	5.0×10^{-12}	2
R41	$RCHO + Br = HBr + RCO3$	$1.8 \times 10^{-11} e^{-460/T}$	2
R42	$GLY + Br = HBr + 2CO + HO2$	$7.7 \times 10^{-12} e^{-580/T}$	2
R43	$MGLY + Br = HBr + CO + MECO3$	$1.8 \times 10^{-11} e^{-460/T}$	2
R44	$BALD + Br = HBr + BZCO3$	$1.8 \times 10^{-11} e^{-460/T}$	2
R45	$ACROLEIN + Br = 0.75FMBR^f + 0.25HBr + 0.25MACO3 + 0.75MGLY + 0.75HO2$	1.0×10^{-11}	2

Table 4. Continued.

No.	Reaction	Reaction rate	Reference
R46	Benzene + Br = Product	1.0×10^{-11}	3
R47	Toluene + Br = Product	1.0×10^{-14}	4
R48	o-xylene + Br = Product	1.6×10^{-14}	4
R49	m-xylene + Br = Product	7.9×10^{-14}	4
R50	p-xylene + Br = Product	4.0×10^{-14}	4
R51	α-pinene + Br = Product	6.8×10^{-14}	5
R52	MACR + Br = Product	3.9×10^{-10}	5
R53	MVK + Br = Product	2.3×10^{-10}	5
R54	MEK + Br = Product	3.6×10^{-10}	5
R55	ETOH + Br = Product	$8.6 \times 10^{-11} e^{45/T}$	5
R56	MEOH + Br = Product	5.5×10^{-11}	5
R57	$Cl + BrCl = Br + Cl_2$	1.45×10^{-11}	6
R58	$Cl + Br_2 = BrCl + Br$	1.94×10^{-10}	7

1 – Sherwen et al. (2016); 2 – Burkholder et al. (2020); 3 – Keefer and Andrews (1950); 4 – Giri et al. (2022); 5 – Li et al. (2021); 6 – Clyne and Cruse (1972); 7 – Khamaganov and Crowley (2010). MB3[a] = $CHBr_3$, MB2[b] = CH_2Br_2, MB2C[c] = CH_2Br_2, MBC2[d] = $CHBr_2Cl$, MBC[e] = CH_2ClBr, FMBR[f] = BrCHO.

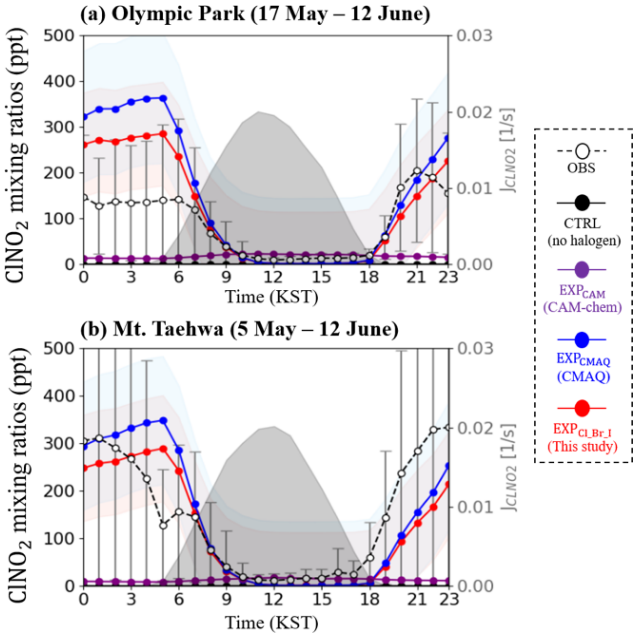

Figure 2. Diurnal variations in the mixing ratios of $ClNO_2$ (unit: ppt) at **(a)** Olympic Park and **(b)** Mount Taehwa stations during the period of the KORUS-AQ campaign. Observed values are represented by open circles (error bars indicate the standard deviation). Colored lines with shaded areas show the hourly averaged mixing ratios of $ClNO_2$ and the corresponding standard deviation from each simulation. The black-shaded area indicates the variations in the photolysis rate of $ClNO_2$ derived from the $EXP_{Cl\_Br\_I}$ simulation.

and $EXP_{Cl\_Br\_I}$ simulations (red dotted line) at two supersites during the period of the KORUS-AQ campaign. Through a sensitivity test, we attempted to identify the key reactions in the $EXP_{Cl\_Br\_I}$ causing differences from the EXP_{CMAQ} simulation. From the studies, we identified four critical halogen reactions: (i) updated reaction rate coefficient of Reaction (R20) in Table 1; (ii) newly added heterogeneous reaction of HOBr as shown in Reaction (R8) of Table 3; (iii) modified parameterization of $\gamma_{N_2O_5}$ as shown in Reaction (R1) of Table 3; and (iv) newly added heterogeneous reaction of NO_2 onto atmospheric aerosols as shown in Reaction (R6) of Table 3. The contributions of these four reactions were calculated and are presented in blue-, green-, yellow-, and red-shaded areas in Fig. 3, respectively. It is evident that the contribution of the parameterization of $\gamma_{N_2O_5}$ is the most significant. A detailed analysis of these differences between EXP_{CMAQ} and the $EXP_{Cl\_Br\_I}$ is further discussed in Table S2.

Figure 3b and d illustrate the contributions of the four reactions to the mixing ratios of $ClNO_2$ at the two supersites. Our results again indicate that selecting the new $\gamma_{N_2O_5}$ led to the largest decreases in the averaged mixing ratios of $ClNO_2$ by 9.58 ppt (50.4 %) and 7.50 ppt (40.3 %) at the Olympic Park and Mount Taehwa stations, respectively. These reductions are obviously attributed to lower values of $\gamma_{N_2O_5}$ in $EXP_{Cl\_Br\_I}$ ($\gamma_{N_2O_5} = \sim 0.013$), compared to those in EXP_{CMAQ} ($\gamma_{N_2O_5} = \sim 0.014$) as shown in Fig. S3. Such a small difference in $\gamma_{N_2O_5}$ led to substantial differences in the mixing ratios of $ClNO_2$. In addition, the inclusion of reaction (recall Reaction R20: $ClO + ClO \rightarrow Cl_2$), with its rate constant reduced by a factor of 10 from the original CMAQ model (see Table S2), led to a 3.40 ppt (17.8 %) decrease in the $ClNO_2$ mixing ratio at the Olympic Park

Table 5. List of homogeneous iodine reactions used in this study.

No.	Reaction	Reaction rate	Reference
R1	$I_2 \xrightarrow{h\nu} 2I$	#1.0/ <I_2>	1
R2	$HOI \xrightarrow{h\nu} I + OH$	#1.0/ <HOI>	1
R3	$IO \xrightarrow{h\nu} I + O^3P$	#1.0/ <IO>	1
R4	$OIO \xrightarrow{h\nu} I$	#1.0/ <OIO>	1
R5	$INO \xrightarrow{h\nu} I + NO$	#1.0/ <INO>	1
R6	$INO_2 \xrightarrow{h\nu} I + NO_2$	#1.0/ <INO_2>	1
R7	$IONO_2 \xrightarrow{h\nu} I + NO_3$	#1.0/ <$IONO_2$>	1
R8	$I_2O_2 \xrightarrow{h\nu} I + OIO$	#1.0/ <$IONO_2$>	1
R9	$I_2O_3 \xrightarrow{h\nu} IO + OIO$	#1.0/ <$IONO_2$>	1
R10	$I_2O_4 \xrightarrow{h\nu} 2OIO$	#1.0/ <$IONO_2$>	1
R11	$CH_3I \xrightarrow{h\nu} I + MEO2$	#1.0/ <CH_3I>	1
R12	$MIC \xrightarrow{h\nu} I + Cl$	#1.0/ <MIC>	1
R13	$MIB \xrightarrow{h\nu} I + Br$	#1.0/ <INO_2>	1
R14	$MI2 \xrightarrow{h\nu} 2I$	#1.0/ <$IONO_2$>	1
R15	$I + O_3 = IO$	$2.1 \times 10^{-11} e^{-830/T}$	2
R16	$I + HO_2 = HI$	$1.5 \times 10^{-11} e^{-1090/T}$	2
R17	$I_2 + OH = HOI + I$	2.1×10^{-10}	1
R18	$HI + OH = I$	$1.6 \times 10^{-11} e^{440/T}$	1
R19	$HOI + OH = IO$	5.0×10^{-12}	1
R20	$IO + HO_2 = HOI$	$1.4 \times 10^{-11} e^{540/T}$	2
R21	$IO + NO = I + NO_2$	$7.15 \times 10^{-12} e^{300/T}$	2
R22	$INO + INO = I_2 + 2NO$	$8.4 \times 10^{-11} e^{-2620/T}$	2
R23	$INO_2 + INO_2 = I_2 + NO_2$	$4.7 \times 10^{-13} e^{-1670/T}$	2
R24	$I_2 + NO_3 = I + IONO_2$	1.5×10^{-12}	2
R25	$IONO_2 + I = I_2 + NO_3$	$9.1 \times 10^{-11} e^{-146/T}$	2
R26	$I + BrO = IO + Br$	1.2×10^{-11}	1
R27	$IO + Br = I + BrO$	2.7×10^{-11}	1
R28	$IO + BrO = Br + I$	$0.3 \times 10^{-11} e^{510/T}$	2
R29	$IO + ClO = I + Cl$	$1.2 \times 10^{-12} e^{280/T}$	2
R30	$OIO + OIO = I_2O_4$	1.5×10^{-10}	2
R31	$OIO + NO = IO + NO_2$	$1.1 \times 10^{-12} e^{542/T}$	2
R32	$IO + IO = 0.4OIO + 0.4I + 0.6I_2O_2$	$5.4 \times 10^{-11} e^{180/T}$	2
R33	$IO + OIO = I_2O_3$	1.5×10^{-10}	2
R34	$I_2O_2 = OIO + I$	$2.5 \times 10^{-14} e^{-9770/T}$	2
R35	$I_2O_4 = 2OIO$	3.8×10^{-2}	2
R36	$INO_2 = NO_2 + I$	$9.9 \times 10^{17} e^{-11\,859/T}$	1
R37	$IONO_2 = NO_2 + IO$	$2.1 \times 10^{15} e^{-13\,670/T}$	1
R38	$CH_3I + OH = HCHO$	$4.3 \times 10^{-12} e^{-1120/T}$	2
R39	$IO + DMS = 0.75SO_2 + 0.25MSA + MEO2$	$3.3 \times 10^{-13} e^{-925/T}$	2
R40	$I + NO = INO$	$k_0 = 1.8 \times 10^{-32}(T/300)^{-1.0}$, $k_\infty = 1.7 \times 10^{-11}(T/300)^{0.0}$, $F = 0.6$ and $N = 1.0$	2
R41	$I + NO_2 = INO_2$	$k_0 = 3.0 \times 10^{31}(T/300)^{-1.0}$, $k_\infty = 6.6 \times 10^{-11}(T/300)^{0.0}$, $F = 0.6$ and $N = 1.0$	2
R42	$IO + NO_2 = IONO_2$	$k_0 = 6.5 \times 10^{-31}(T/300)^{-3.5}$, $k_\infty = 7.6 \times 10^{-12}(T/300)^{-1.5}$, $F = 0.6$ and $N = 1.0$	2
R43	$ICl \xrightarrow{h\nu} I + Cl$	#1.0/ <ICl>	3
R44	$IBr \xrightarrow{h\nu} I + Br$	#1.0/ <IBr>	3
R45	$Cl + I_2 = ICl + I$	2.81×10^{-10}	4
R46	$Br + I_2 = IBr + I$	1.2×10^{-10}	5

1 – Sherwen et al. (2016); 2 – Saiz-Lopez et al. (2014); 3 – Burkholder et al. (2020); 4 – Baklanov et al. (1997); 5 – Bedjanian et al. (1997).

Table 6. Description of the four experiments conducted in this study.

Experiment	Chlorine		Bromine		Iodine	
	Emission	Reaction	Emission	Reaction	Emission	Reaction
CTRL	–	–	–	–	–	–
EXP_{Cl}	✓	✓	–	–	–	–
EXP_{Cl_Br}	✓	✓	✓	✓	–	–
$EXP_{Cl\_Br\_I}$	✓	✓	✓	✓	✓	✓

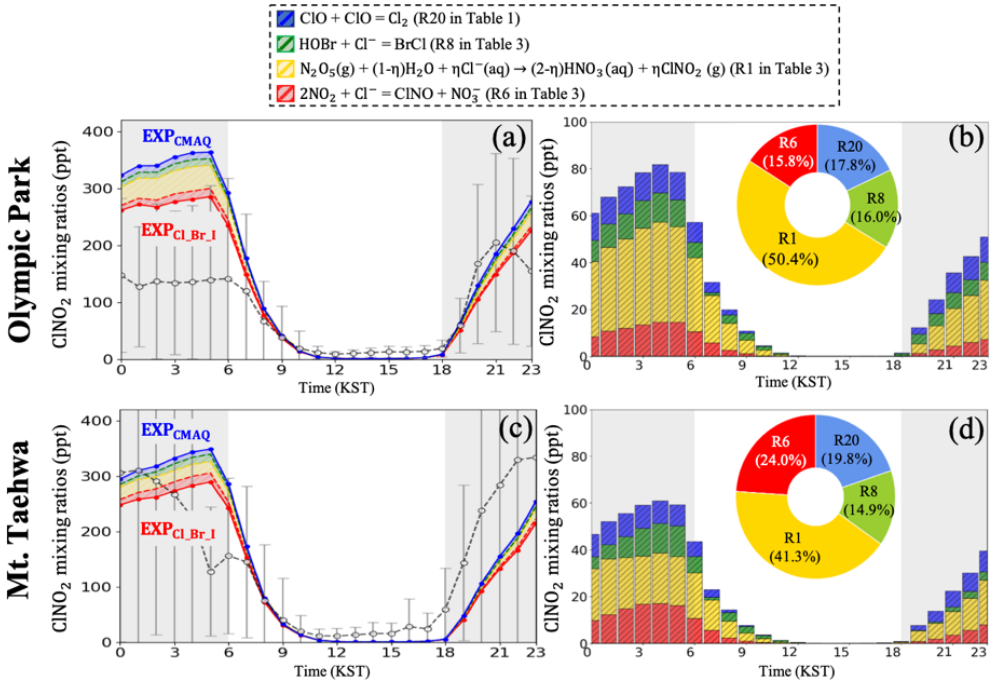

Figure 3. Contributions of halogen reactions to the mixing ratios of $ClNO_2$ in the EXP_{CMAQ} and $EXP_{Cl\_Br\_I}$ simulations at **(a, b)** Olympic Park and **(c, d)** Mount Taehwa stations during the period of the KORUS-AQ campaign. Stacked bars and pie charts show the contributions from four halogen reactions to the mixing ratios of $ClNO_2$. Gray-shaded areas represent nighttime (18:00–06:00 local standard time).

station. This effect is likely due to the slower removal of ClO, which resulted in slightly elevated ClO levels in the boundary layer. The increased ClO may have promoted the formation of $ClONO_2$ (i.e., reservoir species) via reaction with NO_2, thereby reducing the amount of reactive nitrogen available for $ClNO_2$ production through the heterogeneous pathway. Accounting for the heterogeneous reaction of NO_2 and HOBr onto chlorine-containing particles also resulted in reductions in the mixing ratios of $ClNO_2$ by 4.46 ppt (24.0 %) and 2.77 ppt (14.9 %) at the Mount Taehwa station, respectively. These reactions competitively consume chloride-containing particles, thereby reducing the availability of particulate chlorine that is essential for $ClNO_2$ formation. Overall, these results indicate that the reduction in the $ClNO_2$ mixing ratios was primarily driven by the updated chlorine chemistry, particularly the revised parameterization of $\gamma_{N_2O_5}$ and the inclusion of additional chlorine-related reactions, with secondary contributions from bromine chemistry.

Collectively, the four reactions mentioned above may be the key reactions that can significantly change the atmospheric levels of $ClNO_2$. Nevertheless, it should also be noted that the $EXP_{Cl\_Br\_I}$ simulation still exhibited discrepancies with the observed mixing ratios of $ClNO_2$. These remaining biases may be attributed to factors not fully accounted for in the current modeling framework, including (i) the uptake of Cl_2 or related species onto aerosol surfaces, (ii) uncertainties in the $ClNO_2$ yield, (iii) simplified diurnal emissions profiles for HCl and Cl_2, and (iv) missing constrained halogen reactions. These limitations require further targeted sensitivity analyses to better quantify their individual and combined impacts.

Table 7. Statistical metrics for $ClNO_2$ analysis from CTRL, EXP_{CAM}, EXP_{CMAQ}, and $EXP_{Cl\_Br\_I}$ simulations at the Olympic Park and Mount Taehwa stations during the period of the KORUS-AQ campaign.

Target: $ClNO_2$		Olympic Park	Mount Taehwa
	Observed mean (ppt)	85.97	159.36
CTRL	Modeled mean (ppt)	0	0
	MB (ppt)	−85.97	−159.36
	RMSE (ppt)	150.30	288.82
	IOA	0.41	0.40
EXP_{CAM}	Modeled mean (ppt)	17.31	13.49
	MB (ppt)	−68.67	−145.87
	RMSE (ppt)	143.23	281.78
	IOA	0.37	0.40
EXP_{CMAQ}	Modeled mean (ppt)	135.77	152.89
	MB (ppt)	49.80	−6.65
	RMSE (ppt)	204.42	289.19
	IOA	0.62	0.57
$EXP_{Cl\_Br\_I}$	Modeled mean (ppt)	116.76	134.29
	MB (ppt)	30.79	−25.07
	RMSE (ppt)	174.41	272.69
	IOA	0.66	0.59

3.1.3 Uncertainties in Cl_2

Figure 4 represents bar graphs of 24 h averaged Cl_2 mixing ratios from the four experiments, together with the observed Cl_2 mixing ratios at two supersites. Among them, the mixing ratios of Cl_2 from the $EXP_{Cl\_Br\_I}$ agree well with the observed mixing ratios of Cl_2. Based on these findings, we attempted to analyze which reactions contributed to elevated levels of Cl_2. Two key reactions were identified: (i) $HOCl + Cl^- \rightarrow Cl_2$ (Reaction R2 in Table 3) and (ii) $ClONO_2 + Cl^- \rightarrow Cl_2$ (Reaction R3 in Table 3). These reactions accounted for an increase in Cl_2 of 0.18 ppt (14.2 %) and 1.06 ppt (84.1 %), respectively, at the two supersites.

Although the current modeling system has improved the predictions of "campaign-averaged" Cl_2 mixing ratios, it has a serious limitation in reproducing daytime Cl_2 levels, likely due to the extremely fast photo-dissociation rate of Cl_2 (J_{Cl_2} is estimated at 2.5×10^{-3} s^{-1}). In other words, once Cl_2 was produced via daytime halogen reaction pathways (see Reactions R3–R5 in Table 3), it was rapidly removed by the fast photo-dissociation. To address this challenge, several studies suggested potential missing daytime reactions, such as particulate nitrate photolysis and the uptake of O_3 and OH onto atmospheric particles (Peng et al., 2022; Chen et al., 2022). However, these reactions also have limitations in perfectly explaining the relatively high levels of Cl_2 during the daytime. Although the model slightly overestimates Cl_2 mixing ratios during the nighttime (by approximately 0.3 ppt), the major discrepancy lies in the inability to capture daytime peaks. In this context, the accuracy of simulating daytime Cl_2 mixing ratios remains a topic of further discussion.

In addition, significant uncertainties have been reported in observing Cl_2 mixing ratios using the CIMS instrument. The detection limit for Cl_2 in the CIMS instrument was estimated to be 2.9 ppt over a 30 min interval (Jeong et al., 2019). However, the averaged mixing ratios of Cl_2 of 2.08 and 2.69 ppt were measured at Olympic Park and Mount Taehwa, respectively, as depicted in Fig. 4. Given that the observed levels of Cl_2 at the two monitoring stations were very close to the detection limit of the instrument, significant uncertainties likely exist in these measurements of the mixing ratios of Cl_2.

3.1.4 Levels of bromine monoxide (BrO) and iodine monoxide (IO)

To strengthen the model evaluation, we also compared simulated bromine monoxide (BrO) and iodine monoxide (IO) levels with previously reported observational and modeling data, as shown in Fig. 5.

As illustrated in Fig. 5a, several modeling studies reported the mixing ratios of BrO ranging from 0.0 to 1.3 ppt (Koenig et al., 2017; Le Breton et al., 2017; Fan and Li, 2022; Zhu et al., 2019; Li et al., 2020, 2019), which are similar to observed values (Koenig et al., 2017; Peters et al., 2005). Our simulation results indicate relatively low BrO mixing ratios, which may be attributed to low levels of chlorophyll *a* over the Korean Peninsula during May and June (Son, 2013).

For IO, previous field and modeling studies have reported the mixing ratios of IO ranging from 0.0 to 2.5 ppt (Großmann et al., 2013; Allan et al., 2000; Fan and Li, 2022; Li et al., 2020; Takashima et al., 2022; Prados-Roman et al., 2015; Mahajan et al., 2012, 2010; Inamdar et al., 2020). Overall, our simulated IO mixing ratios (0.0–1.8 ppt) over the East Asian ocean region during the KORUS-AQ campaign are comparable to previously reported ranges, as shown in Fig. 5b.

Although BrO and IO were not directly measured during the KORUS-AQ campaign, this comparison suggests that our simulated halogen species are within a reasonable range of previously reported values. These indirect evaluations complement the $ClNO_2$-based validation and enhance confidence in our model's ability to simulate regional-scale behavior of bromine and iodine species.

3.2 Influences of halogen chemistry on O_3 mixing ratios

3.2.1 Comparative analysis at three supersites

Based on the evaluation of model performances, we analyzed the impacts of halogen processes on atmospheric O_3 mixing ratios at three monitoring stations (regarding the locations, see Fig. 1a). Figure 6 represents the diurnal variations in the mixing ratios of O_3 as simulated from both the CTRL (black circles) and $EXP_{Cl\_Br\_I}$ (red circles), together with the observations (white open circles) during the period of the KORUS-

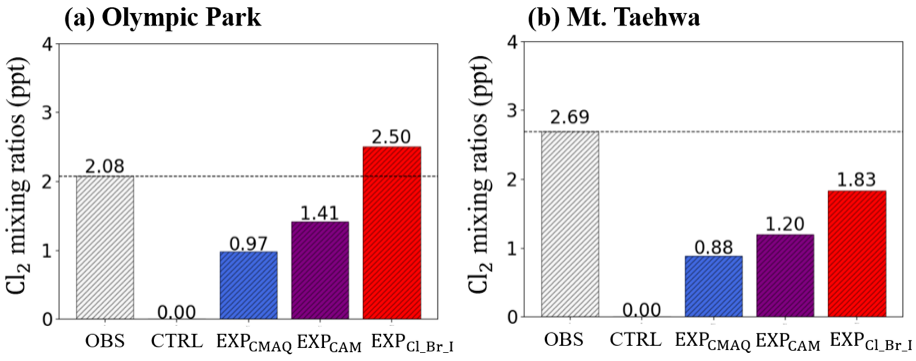

Figure 4. Comparisons of averaged mixing ratios of Cl_2 observed (OBS) and modeled from four simulations (CTRL, EXP_{CMAQ}, EXP_{CAM}, and $EXP_{Cl\_Br\_I}$) at **(a)** Olympic Park and **(b)** Mount Taehwa stations. Dotted lines represent the observed mixing ratios of Cl_2.

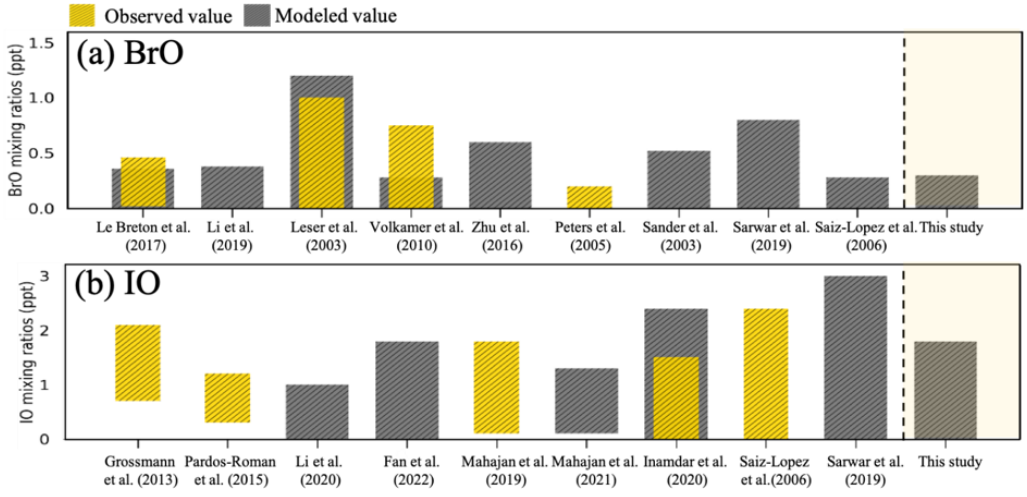

Figure 5. Comparisons between modeled and observed mixing ratios of atmospheric **(a)** BrO and **(b)** IO. Both are observed, and modeled mixing ratios were obtained from the previous studies.

AQ campaign. It shows that the O_3 mixing ratios simulated from the $EXP_{Cl\_Br\_I}$ slightly increased by ∼ 0.06 ppb (0.3 %) and ∼ 0.14 ppb (0.4 %), higher than those from the CTRL at Olympic Park and Mount Taehwa stations, respectively. Similar patterns were also observed in the comparisons between O_3 observations from 320 AIR-KOREA stations and O_3 predictions (as shown in Fig. S4).

It should be noted that the simulated O_3 mixing ratios decreased slightly by ∼ 0.19 ppb (0.3 %), lower than those simulated from the CTRL at the Bangnyung station. These results raised two questions: (i) why did the opposite patterns take place between two land stations and one ocean station (Bangnyung Island station) and (ii) what mechanism caused these opposite patterns in the mixing ratios of O_3? To answer these two questions, we further investigated the role of halogen chemistry in atmospheric O_3 chemistry.

3.2.2 Impacts of halogen processes

Figure 7 illustrates the spatial distributions of the differences between two O_3 mixing ratios simulated under the consideration of individual halogen chemistry over the Korean Peninsula. The CMAQ-simulated O_3 mixing ratios for EXP_{Cl} showed an increase of 0.62 ppb (1.4 %) compared to those from the CTRL over the Korean Peninsula (as shown in Fig. 7a). This increase is attributed to the VOC oxidation by Cl radicals, which leads to the production of additional RO_2 radicals. Additional O_3 is subsequently produced via the $RO_2 + NO$ reactions. It is well-known that VOC oxidation rates by Cl radicals are approximately 10 times faster than those by OH radicals (Edwards and Young, 2024). Several previous studies have also confirmed these findings (Kim et al., 2023; Jo et al., 2023).

Bromine-containing species are known to contribute to O_3 destruction in the atmosphere. However, VOC oxidations by Br radicals also contribute to atmospheric O_3 formation via the reactions of Br+VOC → products+RO_2 (these reactions

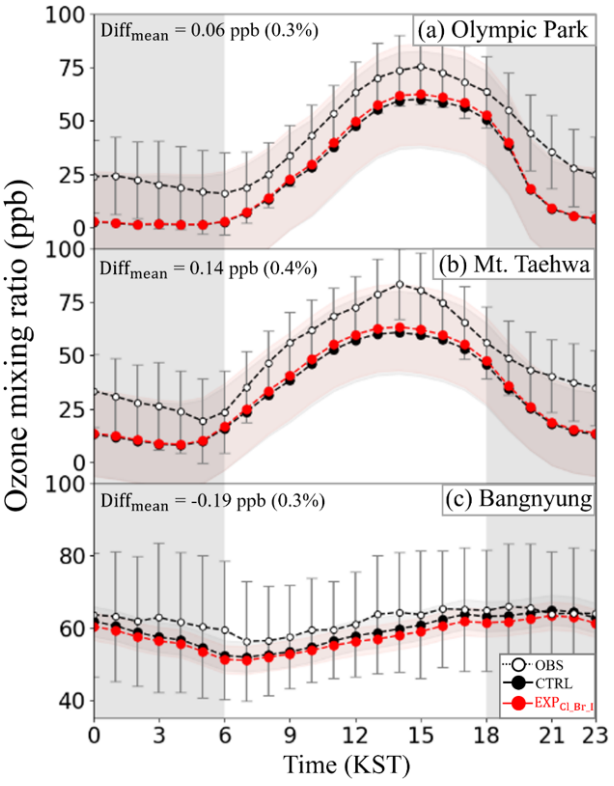

Figure 6. Diurnal variations in the mixing ratios of O_3 from CTRL (black circles) and $EXP_{Cl\_Br\_I}$ (red circles) simulations, together with observed mixing ratios of O_3 (OBS; white circles) at **(a)** Olympic Park, **(b)** Mount Taehwa, and **(c)** Bangnyung stations during the period of the KORUS-AQ campaign. Error bars and shaded areas indicate the standard deviations of observed and modeled O_3, while the gray-shaded areas show the nighttime. $DIFF_{mean}$ represents the difference in the averaged mixing ratios of O_3 between $EXP_{Cl\_Br\_I}$ and CTRL simulations.

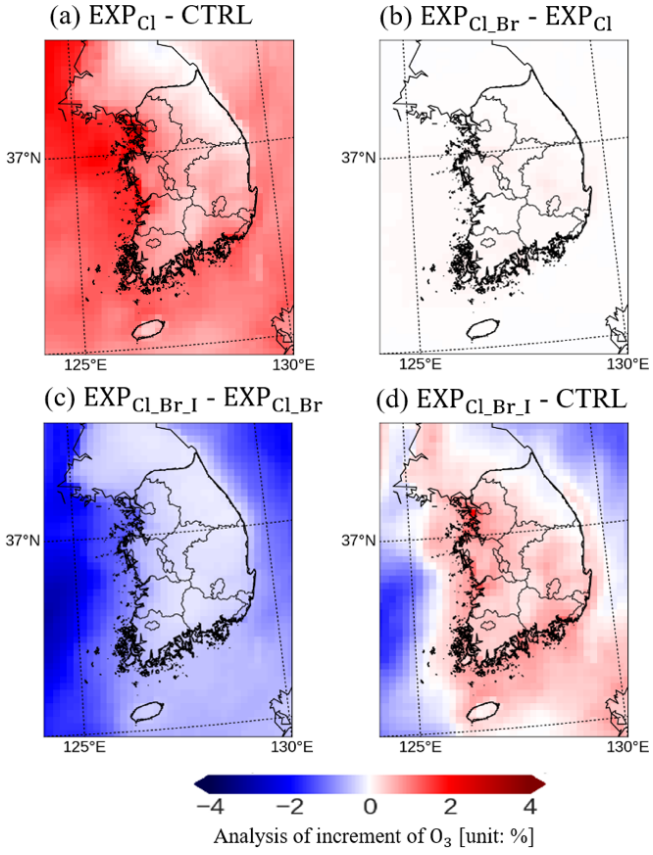

Figure 7. Spatial impacts of **(a)** chlorine processes (EXP_{Cl} − CTRL), **(b)** bromine processes (EXP_{Cl_Br} − EXP_{Cl}), **(c)** iodine processes ($EXP_{Cl\_Br\_I}$ − EXP_{Cl_Br}), and **(d)** total halogen processes ($EXP_{Cl\_Br\_I}$ − CTRL) on O_3 mixing ratios over the Korean Peninsula.

are shown in Reactions R36–R57 in Table 4). As a result, the net effects of bromine processes (i.e., $EXP_{Cl\_Br} - EXP_{Cl}$) lead to a slight increase in O_3 mixing ratios of ∼ 0.01 ppb, as shown in Fig. 7b. This negligible increase is likely due to the competition between O_3 loss via bromine-catalyzed destruction and O_3 production via VOC oxidation.

In Fig. 7c, when iodine processes were incorporated into the modeling system, the surface-averaged O_3 mixing ratios decreased by ∼ 1.39 ppb (2.4 %), particularly over ocean areas. The iodine radicals generated from the photolysis of marine-originated iodine species primarily react with O_3. Given the low levels of VOCs over ocean areas, iodine radicals predominantly participate in the O_3 destruction over the ocean.

Again, the O_3 mixing ratios are controlled by competition between the O_3 production and O_3 destruction. We found that the average O_3 mixing ratios increased by 0.21 ppb (∼ 0.5 %) over land areas and decreased by 0.69 ppb (∼ 1.2 %) over ocean areas under the considerations of entire halogen processes (i.e., $EXP_{Cl\_Br\_I} - CTRL$) (refer to Figs. 7d and S5). These findings are closely in line with the increases in O_3 mixing ratios at the Olympic Park and Mount Taehwa stations (located on land areas) and the decreases in O_3 mixing ratios at the Bangnyung station (located around ocean areas) under the comprehensive considerations of the halogen chemistry, as discussed in Sect. 3.2.1. Such contrasting effects of halogen chemistry between polluted continental and pristine oceanic regions are consistent with previous studies (e.g., Li et al., 2022; Saiz-Lopez et al., 2023), which have also reported O_3 enhancements over land and reductions over the ocean.

3.2.3 Net O_x production

To better understand the influences of the halogen chemistry on atmospheric O_3 mixing ratios, we additionally carried out a quantitative analysis. We calculated O_x production rates ($P(O_x)$) utilizing a definition of expanded O_x family ($\equiv O_3 + O^{1D} + O^{3p} + NO_2 + 2NO_3 + 3N_2O_5 + XNO_2 + XO + XONO_2$; here, X denotes Cl, Br, and I). The constructions of

the $P(O_x)$ are shown in Eqs. (8)–(10):

$$F(O_x) = k_{HO_2+NO}[HO_2][NO] + k_{RO_2+NO}[RO_2][NO] \quad (8)$$

$$\begin{aligned} D(O_x) = {} & k_{NO_2+OH}[NO_2][OH] + k_{O_3+VOC}[O_3][VOC] \\ & + k_{O(^1D)+H_2O}[O(^1D)][H_2O] + k_{O_3+OH}[O_3][OH] \\ & + k_{O_3+HO_2}[O_3][HO_2] + k_{RO_2+NO_2}[RO_2][NO_2] \\ & + (k_{XO+O_3}[O_3] + k_{XO+HO_2}[HO_2] \\ & + k_{XO+O(3p)}[O(^3P)])[XO] \\ & + k_{ClO+NO_2}[NO_2][ClO] + k_{XO+XO}[XO]^2 \\ & + k_{NO_3+VOC}[NO_3][VOC] + 3k_{het}[N_2O_5] \end{aligned} \quad (9)$$

$$P(O_x) = F(O_x) - D(O_x), \quad (10)$$

where $F(O_x)$ and $D(O_x)$ represent the O_x formation rates and O_x destruction rates, respectively. k_i and k_{het} denote the reaction rate constants for reaction i and heterogeneous reactions of N_2O_5, respectively.

Figure 8 shows the average O_x formation rates ($F(O_x)$), O_x destruction rates ($D(O_x)$), and the $P(O_x)$ from the CTRL and $EXP_{Cl\_Br\_I}$ simulations. Over land, rates for reactions of $RO_2 + NO$ and $HO_2 + NO$ in the $F(O_x)$ increased from 2.16 to 2.21 ppb h^{-1} and from 2.05 to 2.09 ppb h^{-1}, respectively, with the full consideration of the halogen processes in the CMAQ model. On the contrary, $D(O_x)$ decreased from 1.12 to 0.97 ppb h^{-1} due to the limited contribution of O_3 destruction by halogen radicals. Consequently, $P(O_x)$ increased from 3.08 to 3.33 ppb h^{-1}. The enhanced $F(O_x)$ of 0.09 ppb h^{-1} with decreased $D(O_x)$ of 0.15 ppb h^{-1} contributes to the increase in $P(O_x)$ of 0.25 ppb h^{-1}. Consistent results were observed at the Olympic Park and Mount Taehwa stations (as shown in Fig. 6a and b).

On the other hand, the $F(O_x)$ decreased by 0.03 ppb h^{-1}, while both $D(O_x)$ and $P(O_x)$ increased by 0.12 and 0.14 ppb h^{-1}, respectively, over the ocean (refer to Fig. 8b and Table 8). This may be caused by the halogen-related losses in $D(O_x)$ (caused mainly by $IO + HO_2$ reaction), significantly contributing to the O_3 destruction. These results indicate that the mixing ratios of O_3 tend to decrease in the presence of iodine radicals over the ocean areas. This is also in line with the case of the Bangnyung station, shown in Fig. 6c.

3.3 Impacts of halogen chemistry on atmospheric species

Figure 9 summarizes the impacts of halogen processes on the mixing ratios of key atmospheric species over/around the Korean Peninsula. The mixing ratios of hydroxyl radicals (OH) and hydroperoxyl radicals (HO_2) increased by ~ 0.002 ppt (2.2 %) and ~ 0.13 ppt (1.6 %), respectively, when including the chlorine processes (i.e., $EXP_{Cl} - CTRL$). This is due to the fact that the chlorine radicals in the atmosphere substitute the role of OH radicals. In other words, chlorine radicals actively react with VOCs. Thus, the VOC mixing ratios

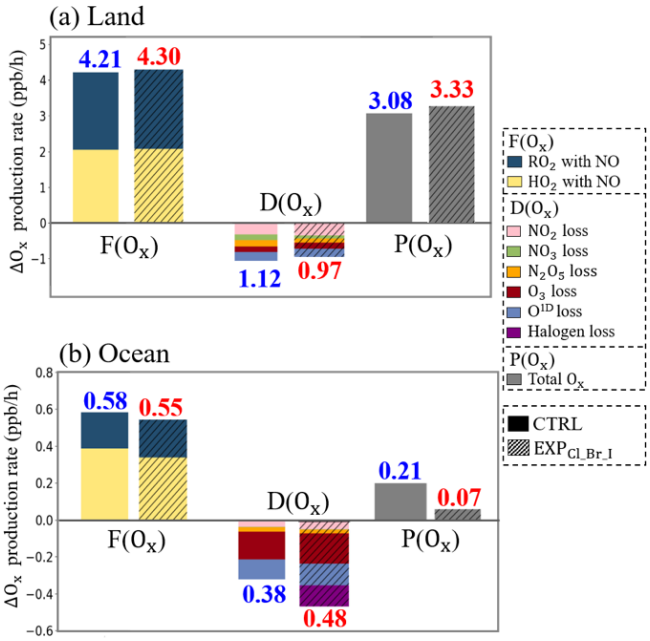

Figure 8. The stacked bar graphs represent O_x formation rate ($F(O_x)$), destruction rate ($D(O_x)$), and production rate ($P(O_x)$) in the CTRL (plain bars) and $EXP_{Cl\_Br\_I}$ (hatched bars) simulations over the **(a)** land and **(b)** ocean areas, respectively, during the period of the KORUS-AQ campaign. Individual reactions contributing to $F(O_x)$ and $D(O_x)$ are indicated by the bar colors.

decreased by 0.39 ppb (1.0 %) due to the active VOC oxidation by Cl radicals. Formaldehyde (HCHO), an intermediate product of VOC oxidation, increased by 0.02 ppb (1.1 %) due to the enhanced rates of the VOC oxidation by Cl radicals. The NO_x mixing ratios also increased by ~ 0.26 ppb (2.6 %). Higher levels of NO_x may be due to the elevated levels of $ClNO_2$, which is a precursor of NO_x in the atmosphere.

We also explored the impacts of bromine processes (i.e., $EXP_{Cl\_Br} - EXP_{Cl}$). The mixing ratios of OH, HO_2, and HCHO further increased by ~ 0.001 ppt (1.1 %), ~ 0.03 ppt (0.4 %), and ~ 0.01 ppb (0.5 %), respectively. These patterns appear to be similar to those in the chlorine case.

The effects of iodine chemistry (i.e., $EXP_{Cl\_Br\_I} - EXP_{Cl\_Br}$) revealed that OH mixing ratios increased by 0.004 ppt (3.1 %). However, the mixing ratios of HO_2 decreased by 0.32 ppt (3.8 %). Interestingly, this increase in OH contrasts with a previous global-scale study (e.g., Li et al., 2022), where iodine chemistry typically leads to lower OH due to halogen-driven O_3 suppression and reduced $O(^1D)$ production. This discrepancy can likely be attributed to differences in the spatial and temporal scales of the analysis. Specifically, our study focuses on a short-term episode (i.e., the KORUS-AQ campaign), during which OH mixing ratios may be more strongly influenced by halogen-mediated radical regeneration. For instance, reactions such as $IO + HO_2 \rightarrow$

Table 8. Averaged budget for O_x formation rates ($F(O_x)$), O_x destruction rates ($D(O_x)$), and O_x production rates ($P(O_x)$) calculated from the CTRL and $EXP_{Cl\_Br\_I}$ simulations during the period of the KORUS-AQ campaign.

	Land		Ocean	
	CTRL	$EXP_{Cl\_Br\_I}$	CTRL	$EXP_{Cl\_Br\_I}$
O_x formation: $F(O_x)$				
$RO_2 + NO$	2.16	2.21	0.20	0.21
$HO_2 + NO$	2.05	2.09	0.39	0.34
Total $F(O_x)$	4.21	4.30	0.58	0.55
O_x destruction: $D(O_x)$				
NO_2 loss[1]	0.33	0.35	0.05	0.04
NO_3 loss[2]	0.17	0.09	< 0.01	< 0.01
N_2O_5 loss[3]	0.20	0.12	0.03	0.02
O_3 loss[4]	0.26	0.24	0.13	0.12
O^{1D} loss[5]	0.16	0.17	0.18	0.17
Halogen loss[6]	0	0.01	0	0.12
Total $D(O_x)$	1.12	0.97	0.38	0.48
Total O_x production: $P(O_x)$				
$P(O_x) = F(O_x) - D(O_x)$	3.08	3.33	0.21	0.07

NO_2 loss[1] = $NO_2 + RO_2$ and $NO_2 + OH$. NO_3 loss[2] = NO_3 + VOC. N_2O_5 loss[3] = Heterogeneous reaction of N_2O_5. O_3 loss[4] = $O_3 + OH$, O_3 + VOC, and $O_3 + HO_2$. O^{1D} loss[5] = $O^{1D} + H_2O$. Halogen loss[6] = $XO + O_3$, HO_2, and O^{3P}; $ClO + NO_2$; XO + XO (where X denotes Cl, Br, and I).

HOI, followed by HOI photolysis (HOI $\xrightarrow{h\nu}$ I+OH), can provide an additional OH source that partially compensates for the O_3-related OH loss. Similar findings have been reported in previous studies (Saiz-Lopez et al., 2012; Mahajan et al., 2021; Stone et al., 2018). The levels of HCHO and VOCs remain almost unchanged due to the fact that iodine radicals do not strongly participate in the reactions with VOCs. The NO_x levels increased slightly by ~ 0.03 ppb (0.3 %) on land and decreased by ~ 0.03 ppb (4.8 %) over ocean areas, which is in line with findings from the previous study (Mahajan et al., 2021).

Collectively, the influence of the full halogen chemistry (i.e., $EXP_{Cl\_Br\_I}$ − CTRL) shows that the OH mixing ratios increased significantly by 0.007 ppt (5.5 %), while the HO_2 mixing ratios decreased by 0.45 ppt (5.3 %) over ocean areas. These patterns are comparable in magnitude to those reported in previous studies. For example, Stone et al. (2018) reported a 2 % increase in OH and a 5 % decrease in HO_2, while Chen et al. (2024) found larger changes with a 12 % increase in OH and an 8 % decrease in HO_2. In addition, Sarwar et al. (2015) found a slight decrease in OH (1 %) accompanied by a more pronounced decrease in HO_2 (11 %). The mixing ratios of HCHO and NO_x increased by ~ 0.03 ppb (1.6 %) and ~ 0.29 ppb (2.9 %) over the land. On the contrary, the mixing ratios of VOCs and NO_x decreased by ~ 0.71 ppb (5.9 %) and ~ 0.05 ppb (7.8 %) over the ocean areas, respectively. The reduction in NO_x over ocean is consistent with Wang et al. (2021), who reported a similar decrease of approximately 6 % due to halogen chemistry.

In addition, elevated oxidant capacity in the simulation of $EXP_{Cl\_Br\_I}$ results in enhancements in the concentrations of sulfate by 0.05 $\mu g\,m^{-3}$ (1.5 %) and secondary organic aerosols by 0.14 $\mu g\,m^{-3}$ (1.8 %). However, concentrations of nitrate and ammonium decreased by $\sim 1.60\,\mu g\,m^{-3}$ (29.4 %) and $\sim 0.55\,\mu g\,m^{-3}$ (5.0 %), respectively, as shown in Fig. S6. This resulted from using smaller uptake coefficient for N_2O_5 (refer to Fig. S3), which suppresses NH_4NO_3 formation. As a result, $PM_{2.5}$ levels decreased from 21.59 to 20.63 $\mu g\,m^{-3}$ (10.5 %) over the Korean Peninsula during the KORUS-AQ campaign.

4 Summary and conclusions

To investigate the impacts of halogen chemistry over the Korean Peninsula, we attempted to add and update reactions involving three halogen species (Cl, Br, and I) in the CMAQ modeling system. First, we estimated anthropogenic emissions of HCl, Cl_2, HBr, and Br_2 from five main sectors (such as industry, residential areas, power plants, solid waste incineration, and others). The anthropogenic emissions for HCl, Cl_2, HBr, and Br_2 were estimated to be 5989.6, 450.8, 460.8, and 240.8 $Mg\,yr^{-1}$ over our research domain, respectively. Second, we also estimated emissions of natural halocarbons and inorganic bromine and iodine (Br_2, I_2, and HOI), based

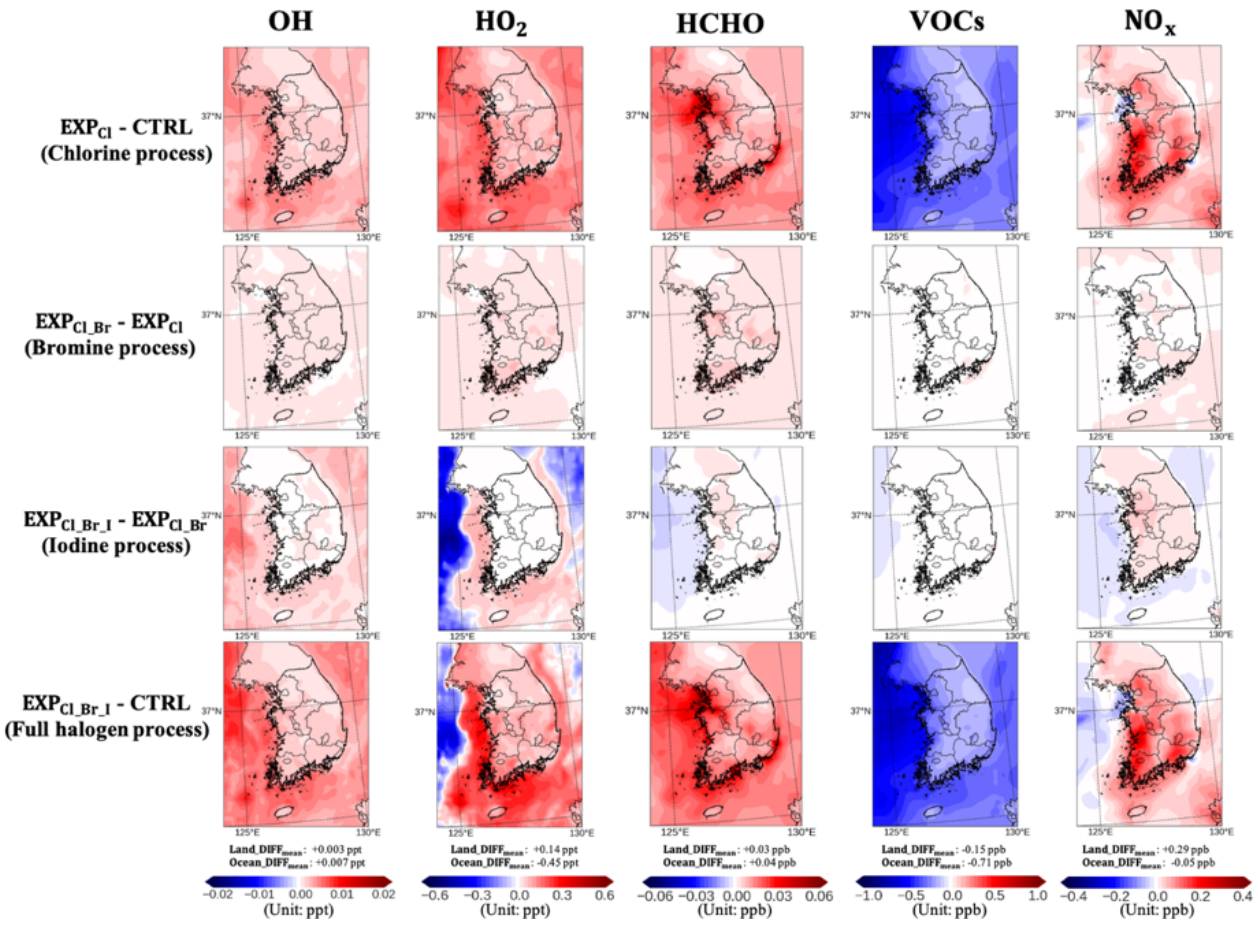

Figure 9. Summaries of the impacts of chlorine processes ($EXP_{Cl} - CTRL$), bromine processes ($EXP_{Cl\_Br} - EXP_{Cl}$), iodine processes ($EXP_{Cl\_Br\_I} - EXP_{Cl\_Br}$), and full halogen processes ($EXP_{Cl\_Br\_I} - CTRL$) on the mixing ratios of OH, HO_2, HCHO, VOCs, and NO_x, respectively, during the period of the KORUS-AQ campaign. Also, $Land\_DIFF_{mean}$ and $Ocean\_DIFF_{mean}$ indicate the differences in the averaged mixing ratios of each species between $EXP_{Cl\_Br\_I}$ and CTRL simulations, over land and ocean, respectively.

on the information derived from the GOCI sensor. Finally, we embedded halogen chemical reactions (58 chlorine reactions, 64 bromine reactions, and 55 iodine reactions) into the CMAQ model.

We then tested the model performances in terms of the mixing ratios of $ClNO_2$ during the period of the KORUS-AQ campaign at two supersites in South Korea. The $EXP_{Cl\_Br\_I}$ simulation exhibited the best performance in terms of the mixing ratios of $ClNO_2$. With the $EXP_{Cl\_Br\_I}$ simulation, the IOA increased from 0.41 to 0.66 at the Olympic Park station and 0.40 to 0.59 at the Mount Taehwa station. Meanwhile, the mean bias (MB) decreased from −85.97 to 30.79 ppt at the Olympic Park station and −159.36 to −25.07 ppt at the Mount Taehwa station. This is because the four following halogen reactions considered in this study contributed to better $ClNO_2$ simulations: (i) $ClO + ClO \rightarrow Cl_2$; (ii) $HOBr + Cl^- \rightarrow BrCl$; (iii) different parameterization of $\gamma_{N_2O_5}$; and (iv) $2NO_2 + Cl^- \rightarrow ClNO + NO_3{}^-$.

In addition to the evaluation of $ClNO_2$, we assessed the overall performance of the implemented halogen chemistry by comparing simulated BrO and IO mixing ratios with previously reported observational and modeling results. The simulated mixing ratios of BrO and IO fall within the reported ranges of 0.0–1.3 ppt for BrO and 0.0–2.5 ppt for IO. This indicates that the updated halogen processes can reasonably reproduce the regional-scale behavior of bromine and iodine species.

Our study further emphasized the significant influences of individual halogen processes on O_3 mixing ratios over South Korea. The average mixing ratios of O_3 increased by ~ 0.21 ppb (0.5 %) over land areas due to the impacts of chlorine and bromine processes. On the contrary, the O_3 mixing ratios decreased by ~ 0.69 ppb (1.2 %) over ocean areas due to iodine processes. In addition, we quantitatively calculated the O_x budget. The net O_x production rate ($P(O_x)$) increased from 3.08 to 3.33 ppb h^{-1} over the land areas and de-

creased from 0.21 to 0.07 ppb h^{-1} over the ocean areas with the simulation of the $EXP_{Cl\_Br\_I}$.

Finally, we further explored the impacts of full halogen processes on the atmospheric composition. Compared with the CTRL simulation, the mixing ratios of HCHO and NO_x increased by ~ 0.03 ppb (1.6 %) and ~ 0.29 ppb (2.9 %) over the land, respectively. On the other hand, the mixing ratios of HO_2 and VOCs decreased by ~ 0.45 ppt (5.3 %) and ~ 0.71 ppb (5.9 %) over the ocean areas, respectively, during the period of the KORUS-AQ campaign.

In conclusion, we believe that we successfully incorporated comprehensive halogen processes into the CMAQ modeling system. Although our evaluation was limited to a few halogen-containing species, the developed framework allowed us to explore the broader impact of halogen chemistry on atmospheric composition and air quality. Despite these contributions, several limitations in modeling fields remain, including (i) the spatiotemporal variability of halogen emissions, (ii) incomplete or uncertain chemical mechanisms, and (iii) limited observational data. In this context, further research is needed to better understand and reduce these uncertainties.

Code and data availability. After user registration, the WRF model 3.8.1 (https://doi.org/10.5065/D6MK6B4K, WRF, 2024, user registration required) and CMAQ v5.2.1 (https://doi.org/10.5281/zenodo.1167892, US EPA Office of Research and Development, 2017) are available from the web pages. The observation data we used can be accessed at https://www-air.larc.nasa.gov/cgi-bin/ArcView/korusaq?GROUND-NIER-OLYMPIC-PARK=1 (NASA, 2019).

Supplement. The supplement related to this article is available online at https://doi.org/10.5194/acp-25-10293-2025-supplement.

Author contributions. Conceptualization: KK, CHS, and KMH. Writing: KK, CHS, and KMH. Experimental design: KK, CHS, KMH, GY, and RB. Supervision: CHS. Validation: KK and CHS. Analysis: KK. Data curation: SK. All authors contributed to this paper for publication.

Competing interests. At least one of the (co-)authors is a member of the editorial board of *Atmospheric Chemistry and Physics*. The peer-review process was guided by an independent editor, and the authors also have no other competing interests to declare.

Disclaimer. Publisher's note: Copernicus Publications remains neutral with regard to jurisdictional claims made in the text, published maps, institutional affiliations, or any other geographical representation in this paper. While Copernicus Publications makes every effort to include appropriate place names, the final responsibility lies with the authors.

Acknowledgements. All authors are grateful for the support of the National Research Foundation of Korea (NRF). We are also grateful for the reviewers' comments, which contributed to enhancing this article.

Financial support. This work was supported by a National Research Foundation of Korea (NRF) grant funded by the Korean government (MSIT) (grant no. 2021R1A2C1006660).

Review statement. This paper was edited by Gunnar Myhre and reviewed by Rafael Pedro Fernandez and one anonymous referee.

References

Abbatt, J. and Waschewsky, G.: Heterogeneous interactions of HOBr, HNO_3, O_3, and NO_2 with deliquescent NaCl aerosols at room temperature, J. Phys. Chem. A, 102, 3719–3725, https://doi.org/10.1021/jp980932d, 1998.

Allan, B. J., McFiggans, G., Plane, J. M., and Coe, H.: Observations of iodine monoxide in the remote marine boundary layer, J. Geophys. Res., 105, 14363–14369, https://doi.org/10.1029/1999JD901188, 2000.

Ammann, M., Cox, R. A., Crowley, J. N., Jenkin, M. E., Mellouki, A., Rossi, M. J., Troe, J., and Wallington, T. J.: Evaluated kinetic and photochemical data for atmospheric chemistry: Volume VI – heterogeneous reactions with liquid substrates, Atmos. Chem. Phys., 13, 8045–8228, https://doi.org/10.5194/acp-13-8045-2013, 2013.

Badia, A., Reeves, C. E., Baker, A. R., Saiz-Lopez, A., Volkamer, R., Koenig, T. K., Apel, E. C., Hornbrook, R. S., Carpenter, L. J., Andrews, S. J., Sherwen, T., and von Glasow, R.: Importance of reactive halogens in the tropical marine atmosphere: a regional modelling study using WRF-Chem, Atmos. Chem. Phys., 19, 3161–3189, https://doi.org/10.5194/acp-19-3161-2019, 2019.

Baklanov, A., Chesnokov, E., and Chichinin, A.: Rate constants for the reactions of molecular iodine with Cl, $SiCl_3$, and SiH3 at 298 K, Int. J. Chem. Kinet., 29, 25–33, https://doi.org/10.1002/(SICI)1097-4601(1997)29:1<25::AID-KIN4>3.0.CO;2-N, 1997.

Bedjanian, Y., Le Bras, G., and Poulet, G.: Kinetics and mechanism of the IO + ClO reaction, J. Phys. Chem. A, 101, 4088–4096, https://doi.org/10.1021/jp963947p, 1997.

Bertram, T. H. and Thornton, J. A.: Toward a general parameterization of N_2O_5 reactivity on aqueous particles: the competing effects of particle liquid water, nitrate and chloride, Atmos. Chem. Phys., 9, 8351–8363, https://doi.org/10.5194/acp-9-8351-2009, 2009.

Burkholder, J., Sander, S., Abbatt, J., Barker, J., Cappa, C., Crounse, J., Dibble, T., Huie, R., Kolb, C., and Kurylo, M.: Chemical kinetics and photochemical data for use in atmospheric studies; evaluation number 19, Nasa panel for data evaluation technical report, 19-5, https://jpldataeval.jpl.nasa.gov/pdf/NASA-JPLEvaluation19-5.pdf (last access: 19 August 2025), 2020.

Byun, D. and Schere, K. L.: Review of the governing equations, computational algorithms, and other components of the Models-

3 Community Multiscale Air Quality (CMAQ) modeling system, Appl. Mech. Rev., 59, 51–77, https://doi.org/10.1115/1.2128636, 2006.

Caram, C., Szopa, S., Cozic, A., Bekki, S., Cuevas, C. A., and Saiz-Lopez, A.: Sensitivity of tropospheric ozone to halogen chemistry in the chemistry–climate model LMDZ-INCA vNMHC, Geosci. Model Dev., 16, 4041–4062, https://doi.org/10.5194/gmd-16-4041-2023, 2023.

Carter, W. P.: Development of the SAPRC-07 chemical mechanism, Atmos. Environ., 44, 5324–5335, https://doi.org/10.1016/j.atmosenv.2010.01.026, 2010.

Chang, W. L., Brown, S. S., Stutz, J., Middlebrook, A. M., Bahreini, R., Wagner, N. L., Dube, W. P., Pollack, I. B., Ryerson, T. B., and Riemer, N.: Evaluating N_2O_5 heterogeneous hydrolysis parameterizations for CalNex 2010, J. Geophys. Res., 121, 5051–5070, https://doi.org/10.1002/2015JD024737, 2016.

Chen, H., Liu, P., Wang, Q., Huang, R., and Sarwar, G.: Impact and pathway of halogens on atmospheric oxidants in coastal city clusters in the Yangtze River Delta region in China, Atmospheric Pollution Research, 15, 101979, https://doi.org/10.1016/j.apr.2023.101979, 2024.

Chen, Q., Xia, M., Peng, X., Yu, C., Sun, P., Li, Y., Liu, Y., Xu, Z., Xu, Z., and Wu, R.: Large daytime molecular chlorine missing source at a suburban site in East China, J. Geophys. Res., 127, e2021JD035796, https://doi.org/10.1029/2021JD035796, 2022.

Clyne, M. and Cruse, H.: Atomic resonance fluorescence spectrometry for rate constants of rapid bimolecular reactions. Part 1. – Reactions $O+NO_2$, $Cl+ClNO$, $Br+ClNO$, J. Chem. Soc. Faraday T., 68, 1281–1299, https://doi.org/10.1039/F29726801281, 1972.

Crawford, J. H., Ahn, J.-Y., Al-Saadi, J., Chang, L., Emmons, L. K., Kim, J., Lee, G., Park, J.-H., Park, R. J., and Woo, J. H.: The Korea–United States air quality (KORUS-AQ) field study, Elem. Sci. Anth., 9, 00163, https://doi.org/10.1525/elementa.2020.00163, 2021.

Deiber, G., George, Ch., Le Calvé, S., Schweitzer, F., and Mirabel, Ph.: Uptake study of $ClONO_2$ and $BrONO_2$ by Halide containing droplets, Atmos. Chem. Phys., 4, 1291–1299, https://doi.org/10.5194/acp-4-1291-2004, 2004.

Deng, S., Shi, Y., Liu, Y., Zhang, C., Wang, X., Cao, Q., Li, S., and Zhang, F.: Emission characteristics of Cd, Pb and Mn from coal combustion: Field study at coal-fired power plants in China, Fuel Process. Technol., 126, 469–475, https://doi.org/10.1016/j.fuproc.2014.06.009, 2014.

Edwards, P. M. and Young, C. J.: Primary Radical Effectiveness: Do the Different Chemical Reactivities of Hydroxyl and Chlorine Radicals Matter for Tropospheric Oxidation?, ACS ES&T Air, 1, 780–788, https://doi.org/10.1021/acsestair.3c00108, 2024.

Evans, M. J. and Jacob, D. J.: Impact of new laboratory studies of N_2O_5 hydrolysis on global model budgets of tropospheric nitrogen oxides, ozone, and OH, Geophys. Res. Lett., 32, L09813, https://doi.org/10.1029/2005GL022469, 2005.

Fan, S. and Li, Y.: The impacts of marine-emitted halogens on OH radicals in East Asia during summer, Atmos. Chem. Phys., 22, 7331–7351, https://doi.org/10.5194/acp-22-7331-2022, 2022.

Fernandez, R. P., Salawitch, R. J., Kinnison, D. E., Lamarque, J.-F., and Saiz-Lopez, A.: Bromine partitioning in the tropical tropopause layer: implications for stratospheric injection, Atmos. Chem. Phys., 14, 13391–13410, https://doi.org/10.5194/acp-14-13391-2014, 2014.

Gantt, B., Sarwar, G., Xing, J., Simon, H., Schwede, D., Hutzell, W. T., Mathur, R., and Saiz-Lopez, A.: The impact of iodide-mediated ozone deposition and halogen chemistry on surface ozone concentrations across the continental United States, Environ. Sci. Technol., 51, 1458–1466, https://doi.org/10.1021/acs.est.6b03556, 2017.

Giri, B. R., Farooq, A., Szőri, M., and Roscoe, J. M.: The kinetics of the reactions of Br atoms with the xylenes: an experimental and theoretical study, Phys. Chem. Chem. Phys., 24, 4843–4858, https://doi.org/10.1039/D1CP03740D, 2022.

Großmann, K., Frieß, U., Peters, E., Wittrock, F., Lampel, J., Yilmaz, S., Tschritter, J., Sommariva, R., von Glasow, R., Quack, B., Krüger, K., Pfeilsticker, K., and Platt, U.: Iodine monoxide in the Western Pacific marine boundary layer, Atmos. Chem. Phys., 13, 3363–3378, https://doi.org/10.5194/acp-13-3363-2013, 2013.

Guenther, A. B., Jiang, X., Heald, C. L., Sakulyanontvittaya, T., Duhl, T., Emmons, L. K., and Wang, X.: The Model of Emissions of Gases and Aerosols from Nature version 2.1 (MEGAN2.1): an extended and updated framework for modeling biogenic emissions, Geosci. Model Dev., 5, 1471–1492, https://doi.org/10.5194/gmd-5-1471-2012, 2012.

Herrmann, M., Schöne, M., Borger, C., Warnach, S., Wagner, T., Platt, U., and Gutheil, E.: Ozone depletion events in the Arctic spring of 2019: a new modeling approach to bromine emissions, Atmos. Chem. Phys., 22, 13495–13526, https://doi.org/10.5194/acp-22-13495-2022, 2022.

Huang, Y., Lu, X., Fung, J. C., Sarwar, G., Li, Z., Li, Q., Saiz-Lopez, A., and Lau, A. K.: Effect of bromine and iodine chemistry on tropospheric ozone over Asia-Pacific using the CMAQ model, Chemosphere, 262, 127595, https://doi.org/10.1016/j.chemosphere.2020.127595, 2021.

Hutzell, W., Luecken, D., Appel, K., and Carter, W.: Interpreting predictions from the SAPRC07 mechanism based on regional and continental simulations, Atmos. Environ., 46, 417–429, https://doi.org/10.1016/j.atmosenv.2011.09.030, 2012.

Iglesias-Suarez, F., Badia, A., Fernandez, R. P., Cuevas, C. A., Kinnison, D. E., Tilmes, S., Lamarque, J.-F., Long, M. C., Hossaini, R., and Saiz-Lopez, A.: Natural halogens buffer tropospheric ozone in a changing climate, Nat. Clim. Change, 10, 147–154, https://doi.org/10.1038/s41558-019-0675-6, 2020.

Inamdar, S., Tinel, L., Chance, R., Carpenter, L. J., Sabu, P., Chacko, R., Tripathy, S. C., Kerkar, A. U., Sinha, A. K., Bhaskar, P. V., Sarkar, A., Roy, R., Sherwen, T., Cuevas, C., Saiz-Lopez, A., Ram, K., and Mahajan, A. S.: Estimation of reactive inorganic iodine fluxes in the Indian and Southern Ocean marine boundary layer, Atmos. Chem. Phys., 20, 12093–12114, https://doi.org/10.5194/acp-20-12093-2020, 2020.

Jeong, D., Seco, R., Gu, D., Lee, Y., Nault, B. A., Knote, C. J., Mcgee, T., Sullivan, J. T., Jimenez, J. L., Campuzano-Jost, P., Blake, D. R., Sanchez, D., Guenther, A. B., Tanner, D., Huey, L. G., Long, R., Anderson, B. E., Hall, S. R., Ullmann, K., Shin, H., Herndon, S. C., Lee, Y., Kim, D., Ahn, J., and Kim, S.: Integration of airborne and ground observations of nitryl chloride in the Seoul metropolitan area and the implications on regional oxidation capacity during KORUS-AQ 2016, Atmos. Chem. Phys., 19, 12779–12795, https://doi.org/10.5194/acp-19-12779-2019, 2019.

Jiang, J., Hao, J., Wu, Y., Streets, D. G., Duan, L., and Tian, H.: Development of mercury emission inventory from coal combustion in China, Environm. Sci., 26, 34–39, https://doi.org/10.13227/j.hjkx.2005.02.007, 2005 (in Chinese).

Jo, H.-Y., Park, J., Heo, G., Lee, H.-J., Jeon, W., Kim, J.-M., Kim, S., Kim, J.-K., Liu, Y., and Liu, P.: Interpretation of the effects of anthropogenic chlorine on nitrate formation over northeast Asia during KORUS-AQ 2016, Sci. Total Environ., 894, 164920, https://doi.org/10.1016/j.scitotenv.2023.164920, 2023.

Keefer, R. and Andrews, L.: The interaction of bromine with benzene and certain of its derivatives, J. Am. Chem. Soc., 72, 4677–4681, https://doi.org/10.1021/ja01166a091, 1950.

Khamaganov, V. and Crowley, J.: Rate coefficients for the reactions $CH_3 + Br_2$ (224–358 K), $CH_3CO + Br_2$ (228 and 298 K), and $Cl + Br_2$ (228 and 298 K), Int. J. Chem. Kinet., 42, 575–585, https://doi.org/10.1002/kin.20505, 2010.

Kim, H., Park, R. J., Kim, S., Jeong, J. I., Jeong, D., Fu, X., and Cho, S.: Effect of nitryl chloride chemistry on air quality in South Korea during the KORUS-AQ campaign, Atmos. Environ., 312, 120045, https://doi.org/10.1016/j.atmosenv.2023.120045, 2023.

Kim, W., Moon, J.-E., Park, Y.-J., and Ishizaka, J.: Evaluation of chlorophyll retrievals from Geostationary Ocean color imager (GOCI) for the north-east Asian region, Remote Sens. Environ., 184, 482–495, https://doi.org/10.1016/j.rse.2016.07.031, 2016.

Koenig, T. K., Volkamer, R., Baidar, S., Dix, B., Wang, S., Anderson, D. C., Salawitch, R. J., Wales, P. A., Cuevas, C. A., Fernandez, R. P., Saiz-Lopez, A., Evans, M. J., Sherwen, T., Jacob, D. J., Schmidt, J., Kinnison, D., Lamarque, J.-F., Apel, E. C., Bresch, J. C., Campos, T., Flocke, F. M., Hall, S. R., Honomichl, S. B., Hornbrook, R., Jensen, J. B., Lueb, R., Montzka, D. D., Pan, L. L., Reeves, J. M., Schauffler, S. M., Ullmann, K., Weinheimer, A. J., Atlas, E. L., Donets, V., Navarro, M. A., Riemer, D., Blake, N. J., Chen, D., Huey, L. G., Tanner, D. J., Hanisco, T. F., and Wolfe, G. M.: BrO and inferred Br_y profiles over the western Pacific: relevance of inorganic bromine sources and a Br_y minimum in the aged tropical tropopause layer, Atmos. Chem. Phys., 17, 15245–15270, https://doi.org/10.5194/acp-17-15245-2017, 2017.

Le Breton, M., Bannan, T. J., Shallcross, D. E., Khan, M. A., Evans, M. J., Lee, J., Lidster, R., Andrews, S., Carpenter, L. J., and Schmidt, J.: Enhanced ozone loss by active inorganic bromine chemistry in the tropical troposphere, Atmos. Environ., 155, 21–28, https://doi.org/10.1016/j.atmosenv.2017.02.003, 2017.

Li, Q., Borge, R., Sarwar, G., de la Paz, D., Gantt, B., Domingo, J., Cuevas, C. A., and Saiz-Lopez, A.: Impact of halogen chemistry on summertime air quality in coastal and continental Europe: application of the CMAQ model and implications for regulation, Atmos. Chem. Phys., 19, 15321–15337, https://doi.org/10.5194/acp-19-15321-2019, 2019.

Li, Q., Zhang, L., Wang, T., Tham, Y. J., Ahmadov, R., Xue, L., Zhang, Q., and Zheng, J.: Impacts of heterogeneous uptake of dinitrogen pentoxide and chlorine activation on ozone and reactive nitrogen partitioning: improvement and application of the WRF-Chem model in southern China, Atmos. Chem. Phys., 16, 14875–14890, https://doi.org/10.5194/acp-16-14875-2016, 2016.

Li, Q., Badia, A., Wang, T., Sarwar, G., Fu, X., Zhang, L., Zhang, Q., Fung, J., Cuevas, C. A., and Wang, S.: Potential effect of halogens on atmospheric oxidation and air quality in China, J. Geophys. Res., 125, e2019JD032058, https://doi.org/10.1029/2019JD032058, 2020.

Li, Q., Fu, X., Peng, X., Wang, W., Badia, A., Fernandez, R. P., Cuevas, C. A., Mu, Y., Chen, J., and Jimenez, J. L.: Halogens enhance haze pollution in China, Environ. Sci. Technol., 55, 13625–13637, https://doi.org/10.1021/acs.est.1c01949, 2021.

Li, Q., Fernandez, R. P., Hossaini, R., Iglesias-Suarez, F., Cuevas, C. A., Apel, E. C., Kinnison, D. E., Lamarque, J.-F., and Saiz-Lopez, A.: Reactive halogens increase the global methane lifetime and radiative forcing in the 21st century, Nat. Commun., 13, 2768, https://doi.org/10.1038/s41467-022-30456-8, 2022.

Liss, P. S., Marandino, C. A., Dahl, E. E., Helmig, D., Hintsa, E. J., Hughes, C., Johnson, M. T., Moore, R. M., Plane, J. M., and Quack, B.: Short-lived trace gases in the surface ocean and the atmosphere, in: Ocean-atmosphere Interactions of Gases and Particles, edited by: Liss, P. and Johnson, M. T., Springer-Verlag GmbH, 1–54, https://doi.org/10.1007/978-3-642-25643-1_1, 2014.

Liu, L., Bei, N., Wu, J., Liu, S., Zhou, J., Li, X., Yang, Q., Feng, T., Cao, J., Tie, X., and Li, G.: Effects of stabilized Criegee intermediates (sCIs) on sulfate formation: a sensitivity analysis during summertime in Beijing–Tianjin–Hebei (BTH), China, Atmos. Chem. Phys., 19, 13341–13354, https://doi.org/10.5194/acp-19-13341-2019, 2019.

Liu, T. and Abbatt, J. P.: An experimental assessment of the importance of S (IV) oxidation by hypohalous acids in the marine atmosphere, Geophys. Res. Lett., 47, e2019GL086465, https://doi.org/10.1029/2019GL086465, 2020.

Liu, Y., Fan, Q., Chen, X., Zhao, J., Ling, Z., Hong, Y., Li, W., Chen, X., Wang, M., and Wei, X.: Modeling the impact of chlorine emissions from coal combustion and prescribed waste incineration on tropospheric ozone formation in China, Atmos. Chem. Phys., 18, 2709–2724, https://doi.org/10.5194/acp-18-2709-2018, 2018.

Mahajan, A. S., Plane, J. M. C., Oetjen, H., Mendes, L., Saunders, R. W., Saiz-Lopez, A., Jones, C. E., Carpenter, L. J., and McFiggans, G. B.: Measurement and modelling of tropospheric reactive halogen species over the tropical Atlantic Ocean, Atmos. Chem. Phys., 10, 4611–4624, https://doi.org/10.5194/acp-10-4611-2010, 2010.

Mahajan, A. S., Gómez Martín, J. C., Hay, T. D., Royer, S.-J., Yvon-Lewis, S., Liu, Y., Hu, L., Prados-Roman, C., Ordóñez, C., Plane, J. M. C., and Saiz-Lopez, A.: Latitudinal distribution of reactive iodine in the Eastern Pacific and its link to open ocean sources, Atmos. Chem. Phys., 12, 11609–11617, https://doi.org/10.5194/acp-12-11609-2012, 2012.

Mahajan, A. S., Li, Q., Inamdar, S., Ram, K., Badia, A., and Saiz-Lopez, A.: Modelling the impacts of iodine chemistry on the northern Indian Ocean marine boundary layer, Atmos. Chem. Phys., 21, 8437–8454, https://doi.org/10.5194/acp-21-8437-2021, 2021.

McDuffie, E. E., Fibiger, D. L., Dube, W. P., Lopez-Hilfiker, F., Lee, B. H., Thornton, J. A., Shah, V., Jaegle, L., Guo, H., and Weber, R. J.: Heterogeneous N_2O_5 uptake during winter: Aircraft measurements during the 2015 WINTER campaign and critical evaluation of current parameterizations, J. Geophys. Res., 123, 4345–4372, https://doi.org/10.1002/2018JD028336, 2018.

NASA: Korea United States Air Quality Study, NASA, https://www-air.larc.nasa.gov/cgi-bin/ArcView/korusaq?

GROUND-NIER-OLYMPIC-PARK=1, (last access: 19 August 2025), 2019.

O'Reilly, J. E. and Werdell, P. J.: Chlorophyll algorithms for ocean color sensors-OC4, OC5 & OC6, Remote Sens. Environ., 229, 32–47, https://doi.org/10.1016/j.rse.2019.04.021, 2019.

Park, M.-O., Shin, W.-C., Son, Y.-B., and Noh, T.-G.: Spatial Variability of in situ and GOCI and MODIS Chlorophyll and CDOM in Summer at the East Sea, Journal of the Korean Society of Marine Environment & Safety, 21, 327–338, https://doi.org/10.7837/kosomes.2015.21.4.327, 2015.

Parrella, J. P., Jacob, D. J., Liang, Q., Zhang, Y., Mickley, L. J., Miller, B., Evans, M. J., Yang, X., Pyle, J. A., Theys, N., and Van Roozendael, M.: Tropospheric bromine chemistry: implications for present and pre-industrial ozone and mercury, Atmos. Chem. Phys., 12, 6723–6740, https://doi.org/10.5194/acp-12-6723-2012, 2012.

Peng, B.-X. and Wu, D.-S.: Distribution and content of bromine in Chinese coals, Journal of Fuel Chemistry and Technology, 42, 769–773, https://doi.org/10.1016/S1872-5813(14)60034-7, 2014.

Peng, X., Wang, T., Wang, W., Ravishankara, A., George, C., Xia, M., Cai, M., Li, Q., Salvador, C. M., and Lau, C.: Photodissociation of particulate nitrate as a source of daytime tropospheric Cl_2, Nat. Commun., 13, 939, https://doi.org/10.6084/m9.figshare.17099252, 2022.

Peters, C., Pechtl, S., Stutz, J., Hebestreit, K., Hönninger, G., Heumann, K. G., Schwarz, A., Winterlik, J., and Platt, U.: Reactive and organic halogen species in three different European coastal environments, Atmos. Chem. Phys., 5, 3357–3375, https://doi.org/10.5194/acp-5-3357-2005, 2005.

Prados-Roman, C., Cuevas, C. A., Hay, T., Fernandez, R. P., Mahajan, A. S., Royer, S.-J., Galí, M., Simó, R., Dachs, J., Großmann, K., Kinnison, D. E., Lamarque, J.-F., and Saiz-Lopez, A.: Iodine oxide in the global marine boundary layer, Atmos. Chem. Phys., 15, 583–593, https://doi.org/10.5194/acp-15-583-2015, 2015.

Pratte, P. and Rossi, M. J.: The heterogeneous kinetics of HOBr and HOCl on acidified sea salt and model aerosol at 40 %–90 % relative humidity and ambient temperature, Phys. Chem. Chem. Phys., 8, 3988–4001, https://doi.org/10.1039/B604321F, 2006.

Qiu, X., Ying, Q., Wang, S., Duan, L., Wang, Y., Lu, K., Wang, P., Xing, J., Zheng, M., and Zhao, M.: Significant impact of heterogeneous reactions of reactive chlorine species on summertime atmospheric ozone and free-radical formation in north China, Sci. Total Environ., 693, 133580, https://doi.org/10.1016/j.scitotenv.2019.133580, 2019a.

Qiu, X., Ying, Q., Wang, S., Duan, L., Zhao, J., Xing, J., Ding, D., Sun, Y., Liu, B., Shi, A., Yan, X., Xu, Q., and Hao, J.: Modeling the impact of heterogeneous reactions of chlorine on summertime nitrate formation in Beijing, China, Atmos. Chem. Phys., 19, 6737–6747, https://doi.org/10.5194/acp-19-6737-2019, 2019b.

Read, K. A., Mahajan, A. S., Carpenter, L. J., Evans, M. J., Faria, B. V., Heard, D. E., Hopkins, J. R., Lee, J. D., Moller, S. J., and Lewis, A. C.: Extensive halogen-mediated ozone destruction over the tropical Atlantic Ocean, Nature, 453, 1232–1235, https://doi.org/10.1038/nature07035, 2008.

Riedel, T. P., Bertram, T. H., Crisp, T. A., Williams, E. J., Lerner, B. M., Vlasenko, A., Li, S.-M., Gilman, J., De Gouw, J., and Bon, D. M.: Nitryl chloride and molecular chlorine in the coastal marine boundary layer, Environ. Sci. Technol., 46, 10463–10470, https://doi.org/10.1021/es204632r, 2012a.

Riedel, T. P., Bertram, T. H., Ryder, O. S., Liu, S., Day, D. A., Russell, L. M., Gaston, C. J., Prather, K. A., and Thornton, J. A.: Direct N_2O_5 reactivity measurements at a polluted coastal site, Atmos. Chem. Phys., 12, 2959–2968, https://doi.org/10.5194/acp-12-2959-2012, 2012b.

Riemer, N., Vogel, H., Vogel, B., Schell, B., Ackermann, I., Kessler, C., and Hass, H.: Impact of the heterogeneous hydrolysis of N_2O_5 on chemistry and nitrate aerosol formation in the lower troposphere under photosmog conditions, J. Geophys. Res.-Atmos., 108, 4144, https://doi.org/10.1029/2002JD002436, 2003.

Roberts, J. M., Osthoff, H. D., Brown, S. S., Ravishankara, A., Coffman, D., Quinn, P., and Bates, T.: Laboratory studies of products of N_2O_5 uptake on Cl- containing substrates, Geophys. Res. Lett., 36, L20808, https://doi.org/10.1029/2009GL040448, 2009.

Saiz-Lopez, A., Lamarque, J.-F., Kinnison, D. E., Tilmes, S., Ordóñez, C., Orlando, J. J., Conley, A. J., Plane, J. M. C., Mahajan, A. S., Sousa Santos, G., Atlas, E. L., Blake, D. R., Sander, S. P., Schauffler, S., Thompson, A. M., and Brasseur, G.: Estimating the climate significance of halogen-driven ozone loss in the tropical marine troposphere, Atmos. Chem. Phys., 12, 3939–3949, https://doi.org/10.5194/acp-12-3939-2012, 2012.

Saiz-Lopez, A., Fernandez, R. P., Ordóñez, C., Kinnison, D. E., Gómez Martín, J. C., Lamarque, J.-F., and Tilmes, S.: Iodine chemistry in the troposphere and its effect on ozone, Atmos. Chem. Phys., 14, 13119–13143, https://doi.org/10.5194/acp-14-13119-2014, 2014.

Saiz-Lopez, A., Fernandez, R. P., Li, Q., Cuevas, C. A., Fu, X., Kinnison, D. E., Tilmes, S., Mahajan, A. S., Gomez Martin, J. C., and Iglesias-Suarez, F.: Natural short-lived halogens exert an indirect cooling effect on climate, Nature, 618, 967–973, https://doi.org/10.1038/s41586-023-06119-z, 2023.

Sander, S., Friedl, R., Golden, D., Kurylo, M., Moortgat, G., Wine, P., Ravishankara, A., Kolb, C., Molina, M., and Finlyason-Pitts, B.: Chemical kinetics and photochemical data for use in atmospheric studies: Evaluation number 15, Jet Propulsion Laboratory, California Institute of Technology, Pasadena, CA, 2010.

Sarwar, G., Simon, H., Bhave, P., and Yarwood, G.: Examining the impact of heterogeneous nitryl chloride production on air quality across the United States, Atmos. Chem. Phys., 12, 6455–6473, https://doi.org/10.5194/acp-12-6455-2012, 2012.

Sarwar, G., Gantt, B., Schwede, D., Foley, K., Mathur, R., and Saiz-Lopez, A.: Impact of enhanced ozone deposition and halogen chemistry on tropospheric ozone over the Northern Hemisphere, Environ. Sci. Technol., 49, 9203–9211, https://doi.org/10.1021/acs.est.5b01657, 2015.

Sarwar, G., Gantt, B., Foley, K., Fahey, K., Spero, T. L., Kang, D., Mathur, R., Foroutan, H., Xing, J., and Sherwen, T.: Influence of bromine and iodine chemistry on annual, seasonal, diurnal, and background ozone: CMAQ simulations over the Northern Hemisphere, Atmos. Environ., 213, 395–404, https://doi.org/10.1016/j.atmosenv.2019.06.020, 2019.

Sherwen, T., Evans, M. J., Carpenter, L. J., Andrews, S. J., Lidster, R. T., Dix, B., Koenig, T. K., Sinreich, R., Ortega, I., Volkamer, R., Saiz-Lopez, A., Prados-Roman, C., Mahajan, A. S., and Ordóñez, C.: Iodine's impact on tropospheric oxidants: a global

model study in GEOS-Chem, Atmos. Chem. Phys., 16, 1161–1186, https://doi.org/10.5194/acp-16-1161-2016, 2016.

Simpson, W. R., Brown, S. S., Saiz-Lopez, A., Thornton, J. A., and von Glasow, R.: Tropospheric halogen chemistry: Sources, cycling, and impacts, Chem. Rev., 115, 4035–4062, https://doi.org/10.1021/cr5006638, 2015.

Skamarock, W. C., Klemp, J. B., Dudhia, J., Gill, D. O., Barker, D. M., Duda, M. G., Huang, X.-Y., Wang, W., and Powers, J. G.: A description of the advanced research WRF version 3, NCAR technical note, 475, https://doi.org/10.5065/D68S4MVH, 2008.

Slusher, D. L., Huey, L. G., Tanner, D. J., Flocke, F. M., and Roberts, J. M.: A thermal dissociation–chemical ionization mass spectrometry (TD-CIMS) technique for the simultaneous measurement of peroxyacyl nitrates and dinitrogen pentoxide, J. Geophys. Res., 109, D19315, https://doi.org/10.1029/2004JD004670, 2004.

Son, H.-J.: Long-term variations of phytoplankton biomass and water quality in the downstream of Nakdong River, Journal of Korean Society of Environmental Engineers, 35, 263–267, https://doi.org/10.4491/KSEE.2024.46.11.687, 2013.

Stone, D., Sherwen, T., Evans, M. J., Vaughan, S., Ingham, T., Whalley, L. K., Edwards, P. M., Read, K. A., Lee, J. D., Moller, S. J., Carpenter, L. J., Lewis, A. C., and Heard, D. E.: Impacts of bromine and iodine chemistry on tropospheric OH and HO_2 : comparing observations with box and global model perspectives, Atmos. Chem. Phys., 18, 3541–3561, https://doi.org/10.5194/acp-18-3541-2018, 2018.

Takashima, H., Kanaya, Y., Kato, S., Friedrich, M. M., Van Roozendael, M., Taketani, F., Miyakawa, T., Komazaki, Y., Cuevas, C. A., Saiz-Lopez, A., and Sekiya, T.: Full latitudinal marine atmospheric measurements of iodine monoxide, Atmos. Chem. Phys., 22, 4005–4018, https://doi.org/10.5194/acp-22-4005-2022, 2022.

US EPA Office of Research and Development: CMAQ (Version 5.2), Zenodo, https://doi.org/10.5281/zenodo.1167892, 2017.

von Glasow, R. and Crutzen, P.: Tropospheric Halogen Chemistry, in: Treatise on Geochemistry, edited by: Holland, H. D. and Turekian, K. K., Pergamon, Oxford, ISBN 9780080450919, 2007.

Wang, X., Wang, H., Xue, L., Wang, T., Wang, L., Gu, R., Wang, W., Tham, Y. J., Wang, Z., and Yang, L.: Observations of N_2O_5 and $ClNO_2$ at a polluted urban surface site in North China: High N_2O_5 uptake coefficients and low $ClNO_2$ product yields, Atmos. Environ., 156, 125–134, https://doi.org/10.1016/j.atmosenv.2017.02.035, 2017.

Wang, X., Jacob, D. J., Downs, W., Zhai, S., Zhu, L., Shah, V., Holmes, C. D., Sherwen, T., Alexander, B., Evans, M. J., Eastham, S. D., Neuman, J. A., Veres, P. R., Koenig, T. K., Volkamer, R., Huey, L. G., Bannan, T. J., Percival, C. J., Lee, B. H., and Thornton, J. A.: Global tropospheric halogen (Cl, Br, I) chemistry and its impact on oxidants, Atmos. Chem. Phys., 21, 13973–13996, https://doi.org/10.5194/acp-21-13973-2021, 2021.

Wiedinmyer, C., Akagi, S. K., Yokelson, R. J., Emmons, L. K., Al-Saadi, J. A., Orlando, J. J., and Soja, A. J.: The Fire INventory from NCAR (FINN): a high resolution global model to estimate the emissions from open burning, Geosci. Model Dev., 4, 625–641, https://doi.org/10.5194/gmd-4-625-2011, 2011.

Woo, J.-H., Kim, Y., Kim, H.-K., Choi, K.-C., Eum, J.-H., Lee, J.-B., Lim, J.-H., Kim, J., and Seong, M.: Development of the CREATE inventory in support of integrated climate and air quality modeling for Asia, Sustainability-Basel, 12, 7930, https://doi.org/10.3390/su12197930, 2020.

WRF: WRF User Page, WRF [code], https://doi.org/10.5065/D6MK6B4K, 2024.

Yang, X., Cox, R. A., Warwick, N. J., Pyle, J. A., Carver, G. D., O'Connor, F. M., and Savage, N. H.: Tropospheric bromine chemistry and its impacts on ozone: A model study, J. Geophys. Res., 110, D23311, https://doi.org/10.1029/2005JD006244, 2005.

Yi, X., Yin, S., Huang, L., Li, H., Wang, Y., Wang, Q., Chan, A., Traore, D., Ooi, M. C. G., and Chen, Y.: Anthropogenic emissions of atomic chlorine precursors in the Yangtze River Delta region, China, Sci. Total Environ., 771, 144644, https://doi.org/10.1016/j.scitotenv.2020.144644, 2021.

Yu, C., Wang, Z., Xia, M., Fu, X., Wang, W., Tham, Y. J., Chen, T., Zheng, P., Li, H., Shan, Y., Wang, X., Xue, L., Zhou, Y., Yue, D., Ou, Y., Gao, J., Lu, K., Brown, S. S., Zhang, Y., and Wang, T.: Heterogeneous N_2O_5 reactions on atmospheric aerosols at four Chinese sites: improving model representation of uptake parameters, Atmos. Chem. Phys., 20, 4367–4378, https://doi.org/10.5194/acp-20-4367-2020, 2020.

Zhu, L., Jacob, D. J., Eastham, S. D., Sulprizio, M. P., Wang, X., Sherwen, T., Evans, M. J., Chen, Q., Alexander, B., Koenig, T. K., Volkamer, R., Huey, L. G., Le Breton, M., Bannan, T. J., and Percival, C. J.: Effect of sea salt aerosol on tropospheric bromine chemistry, Atmos. Chem. Phys., 19, 6497–6507, https://doi.org/10.5194/acp-19-6497-2019, 2019.